

Breaking time reversal symmetry in chaotic driven Rydberg atoms

Krzysztof Sacha^{1,2}, Jakub Zakrzewski², and Dominique Delande³

¹ *Fachbereich Physik, Universität Marburg,
Renthof 6, D-35032 Marburg, Germany*

² *Instytut Fizyki imienia Mariana Smoluchowskiego, Uniwersytet Jagielloński,
ulica Reymonta 4, PL-30-059 Kraków, Poland*

³ *Laboratoire Kastler-Brossel, Tour 12, Étage 1, Université Pierre et Marie Curie,
4 Place Jussieu, 75005 Paris, France*

(October 30, 2018)

Abstract

We consider the dynamics of Rydberg states of the hydrogen atom driven by a microwave field of elliptical polarization, with a possible additional static electric field. We concentrate on the effect of a resonant weak field - whose frequency is close to the Kepler frequency of the electron around the nucleus - which essentially produces no ionization of the atom, but completely mixes the various states inside an hydrogenic manifold of fixed principal quantum number. For sufficiently small fields, a perturbative approach (both in classical and quantum mechanics) is relevant. For some configurations of the fields, the classical secular motion (i.e. evolution in time of the elliptical electronic trajectory) is shown to be predominantly chaotic. Changing the orientation of the static field with respect to the polarization of the microwave field allows us to investigate the effect of generalized time-reversal symmetry breaking on the statistical properties of energy levels.

I. INTRODUCTION

Sixteen years ago, Bohigas, Giannoni and Schmit, in a seminal paper [1], formulated the conjecture that quantum systems which are chaotic in the classical limit, generically have statistical properties of energy levels described by Random Matrix Theory (RMT) [2]. While RMT had proven useful in characterizing nuclear spectra [3], the conjecture was quite surprising since it claimed an applicability of RMT statistics to deterministic systems with very few degrees of freedom. While some counterexamples exist (see e.g. [4]), the conjecture remains widely accepted and played a very stimulating role in quantum chaos studies (see for reviews [5,6]).

Depending on the symmetries of a given strongly chaotic system, the statistical properties of its quantum spectrum fall into one of the three classes known from RMT: orthogonal, unitary and symplectic. The orthogonal class is associated with Hamiltonians invariant with respect to some anti-unitary symmetry. Typically this is true for time-reversal invariant systems, but also for more complicated anti-unitary symmetry (generalized time-reversal symmetry) as the product of a time-reversal with some discrete reflection. Roughly speaking, this happens if a basis can be chosen where the matrix elements of the Hamiltonian are all real. The corresponding statistical ensemble of (real symmetric) random matrices is referred to as the Gaussian Orthogonal Ensemble (GOE). In the absence of any anti-unitary symmetry, the corresponding class of complex hermitian matrices is known as the Gaussian Unitary Ensemble (GUE). Finally, specific considerations apply to half-integer spin systems with (generalized) time-reversal symmetry. Indeed, the energy levels of these systems are systematically two-fold degenerate (this is the well-known Kramers degeneracy). In the presence of a geometrical symmetry like azimuthal symmetry, the Kramers degeneracy is hidden and the GOE statistics apply. With no geometrical symmetries, the Gaussian Symplectic Ensemble (GSE) has to be used. All these three classes of systems are characterized by level repulsion, that is zero probability of observing accidentally degenerate energy levels. This is to be contrasted with a generic behaviour of multidimensional integrable systems where close lying levels are uncorrelated and obey a Poisson statistics [7]. For a generic Hamiltonian system, where typically chaotic and regular motions coexist, the statistical properties of energy levels are not universal and are expected to be intermediate between the two limiting cases, Poisson and RMT.

While the conjecture has been tested on a number of theoretical models (we refer the reader to reviews [5,6] rather than numerous original papers), experimental verifications are much less abundant and restricted fully, as far as we know, to the orthogonal universality class [8]. This is probably due to the fact that most experimental results are obtained for atomic and molecular spectra. In the presence of a uniform magnetic field, the time-reversal symmetry is broken, but a anti-unitary symmetry persists [5]. Thus, observing GUE statistics should require well controlled inhomogeneous fields on the atomic scale, which has not been achieved.

An alternative is to study the eigenmodes not of the Schrödinger equation, but of a different although similar wave equation. The best examples are two-dimensional microwave billiards (in fact three-dimensional flat cavities below the cut-off frequency) where the classical Helmholtz wave equation is in fact equivalent to the time-independent Schrödinger equation. There, breaking of the time reversal invariance is possible by using magnetic de-

vices and GUE-type statistics have been observed experimentally [9,10]. Still it is desirable to have at hand a quantum system where manifestations of the generalized time reversal symmetry breaking is experimentally accessible. The aim of this paper is to discuss an example of such a system. As mentioned above, breaking all anti-unitary symmetries using static fields is not possible. Hence, the idea is to use a time-dependent field acting on an atom. With an oscillatory field alone, the product of time reversal by symmetry with respect to one of the polarization axis is an anti-unitary symmetry. Hence, GUE statistics requires to combine a microwave field and a static field.

The model we use, the Rydberg states of the hydrogen atom driven by a microwave field, has a long history of its own. The system attracted attention when it turned out that experimental results [11] on the ionization probability as a function of the microwave field and frequency could be explained in terms of the underlying classical chaotic dynamics which results in a diffusive energy gain of the Rydberg electron and eventually to ionization [12]. Many interesting phenomena (e.g. quantum localization) have been studied on this model both theoretically and experimentally (see e.g. review papers [13–16]). The first experiments involved linearly polarized microwaves allowing for a rough description of the ionization thresholds via a simple one-dimensional time-dependent model where the motion of the electron is restricted to the microwave field axis [17]. For other polarizations (available in recent experiments [18,19]), such a simple model is not possible: the simplest dynamics may be two-dimensional where the electronic motion is restricted to the polarization plane. Such models have been investigated both for circular polarization (CP) [20–22] and general elliptical polarization (EP) [23–25].

When not only the ionization thresholds, but also the more subtle details of the dynamics, have to be studied, a full three dimensional atom must be considered. For LP microwave, the conservation of the angular momentum projection onto the polarization axis, L_z , makes the dynamics effectively two-dimensional and time dependent. For CP case, while L_z is not conserved, the transformation to the frame rotating with the microwave frequency removes the explicit oscillatory time-dependence, leading to a three-dimensional time independent problem. Both these simplifications are no longer possible in the general EP microwave field and the problem becomes truly three dimensional and time dependent, providing new challenges to the theory. It is this situation which we shall consider later on.

However, instead of discussing typical “large” microwave amplitude for fields which lead to an efficient excitation of Rydberg atoms to higher excited states and finally to ionization, we shall consider a “weak” perturbation of an atom where the exchange of energy between the field and the atom is negligible. The fact that the Coulomb problem is highly degenerate provides us with the possibility, as shown below, to reach chaotic dynamics even for infinitesimally weak external fields. This is not in contradiction with the Kolmogorov-Arnold-Moser (KAM) theorem [26] since the latter precisely does not apply for degenerate situations. Those weak fields do not really excite the atom, but rather couple and mix among each other the n_0^2 states of a degenerate hydrogenic manifold with a given principal quantum number n_0 . The degeneracy is lifted, states undergo small (but measurable) shifts that reflect the dynamics of the n_0 manifold. Such a situation is referred to as intramanifold dynamics (by contrast to a typical intermanifold coupling leading to atomic excitation and ionization). An intramanifold chaotic behaviour is quite attractive from the theoretical point of view. It yields an effective quantum Hamiltonian acting in the n_0 space, whose

eigenvalues are the energy shifts, and is represented by a *finite* dimensional matrix of size n_0^2 (modulo the remaining point symmetries) with no cutoff errors. The semiclassical limit is realized by letting $n_0 \rightarrow \infty$.

The first attempt to produce some intramanifold chaos used the hydrogen atom in uniform crossed magnetic and electric fields [27,28], which was later extended to arbitrary mutual orientations of the two fields [29]. The authors, exploring second order perturbation theory, have observed signatures of intramanifold chaos in the quantum spectrum. However, the situation is somewhat complex: the first order term (in the two external fields) is always integrable; it is only when combined with a second order term of a comparable magnitude that some noticeable region of chaos can be created. But this implies the application of large fields, and higher order terms in the perturbative expansion are of importance. That, unfortunately, has been neglected by the authors. Moreover, the high electric field values used lead then to an extremely fast field ionization which blurs any long-time effects in the dynamics. Especially, there are no more bound states in these conditions, but only broad overlapping resonances, which implies that the statistical properties cannot be described by one of the three standard ensembles of random matrices [30].

Recently, we have proposed [31] another system revealing chaotic intramanifold dynamics which does not suffer from the mentioned deficiency. This is an hydrogen atom driven resonantly (i.e. with the frequency ω which is an integer multiple of the Kepler frequency $\omega_K = 1/n_0^3$) by an elliptically polarized microwave with the possible addition of some static weak electric field. The latter allows us to break any generalized time-reversal symmetry of the system.

Since the driving field is periodic, by applying the Floquet theorem, one can find the eigenstates of the system (the so-called Floquet or dressed states). The eigenenergies of the system are referred to as quasienergies of the system and are defined modulo $\hbar\omega$. As we have discussed shortly for a 2 : 1 resonance [31], the statistical properties of the quasienergies reveal convincingly the symmetry breaking. Here we discuss the same system, i.e. an hydrogen atom driven by a resonant EP microwave field, both in the presence and in the absence of the static field.

The paper is organized as follows. In Sec. II we derive the quantum perturbative Hamiltonian for our system and its semiclassical counterpart. They are used in Sec. III to analyze the behavior of the atom in a pure microwave field and in Sec. IV for a microwave field combined with a static electric field. The summary and the future perspectives form the content of the concluding section.

II. PERTURBATION APPROACH

We consider a realistic three-dimensional hydrogen atom placed in a static electric field and driven by an elliptically polarized microwave field. We define the z -axis as perpendicular to the plane of the polarization of the microwave field. The Hamiltonian of the system, in atomic units, neglecting relativistic effects, assuming infinite mass of the nucleus, and employing dipole approximation reads:

$$H = \frac{\mathbf{p}^2}{2} - \frac{1}{r} + F(x \cos \omega t + \alpha y \sin \omega t) + \mathbf{E} \cdot \mathbf{r}, \quad (2.1)$$

where F , α and ω stand, respectively, for the amplitude, degree of elliptical polarization and frequency of the microwave field while \mathbf{E} denotes the static electric field.

As mentioned in the Introduction, we are interested in effects due to weak external fields. In the absence of any external field, the energy levels of the system are $-1/2n_0^2$ with n_0 the principal quantum number; the degeneracy of the n_0 hydrogenic manifold is n_0^2 . Even very weak fields mix strongly states within the manifold; on the other hand, it is perfectly justified to treat coupling to other manifolds perturbatively. We shall do so first quantum-mechanically with the help of the effective Hamiltonian approach [32]. Then, we construct its (semi-)classical equivalent. The latter allows us to study the character of the classical motion and search for parameters corresponding to chaotic dynamics.

A. Quantum perturbation method

For any time-periodic Hamiltonian, the Floquet theorem states that the most general solution of the Schrödinger equation can be written as a linear combination of the “Floquet states”, which are time-periodic functions and eigenstates of the so-called Floquet Hamiltonian $\mathcal{H}_{\text{Floquet}}$ [33] of the system:

$$\mathcal{H}_{\text{Floquet}} |\phi(t)\rangle = \left(H - i \frac{\partial}{\partial t} \right) |\phi(t)\rangle = \epsilon |\phi(t)\rangle \quad (2.2)$$

where ϵ and $|\phi(t)\rangle$ are respectively the quasienergy and the Floquet state. The solutions of Eq. (2.2) have to satisfy the usual boundary conditions in configuration space and periodic boundary condition in the time coordinate (by construction, Floquet states are time-periodic). Hence, the Floquet Hamiltonian $\mathcal{H}_{\text{Floquet}}$ acts on an extended Hilbert space containing also the time coordinate.

For studying the quasi-energy spectrum, is it convenient to choose, as a basis of the atomic Hilbert space, the Sturmian functions (see e.g. [34–36] for details of this application) $|n, L, M\rangle^{(\Lambda)}$, where L and M are the usual angular and magnetic quantum numbers respectively while $n \geq L + 1$ labels the radial functions whose number of nodes is $n - L - 1$. Λ is a scaling parameter (unit of length in configuration space) for the Sturmian functions. For $\Lambda = n_0$, the Sturmian functions with $n = n_0$ are the exact hydrogenic states, eigenstates of the unperturbed atom. As we intend to describe the dynamics inside the n_0 -manifold of the hydrogen atom, we choose to keep $\Lambda = n_0$ in all calculations.

Along the time coordinate, we choose the usual oscillating exponential functions as a basis of time-periodic functions. They are labeled with an integer index K and defined by:

$$\langle t|K\rangle = e^{-iK\omega t} \quad (2.3)$$

The whole Hilbert space of the atom + periodic perturbation system (Floquet Hamiltonian) is spanned by the tensor product of the configuration space and time basis:

$$|n, L, M, K\rangle = |n, L, M\rangle^{(n_0)} \otimes |K\rangle. \quad (2.4)$$

In the dressed atom language, K may be loosely identified with the number of photons exchanged between the atom and the field.

The Sturmian basis is not orthogonal, but it satisfies the following relation:

$$\sum_{n,L,M,K} |n, L, M, K\rangle \langle n, L, M, K| \frac{1}{2r} = 1 \quad (2.5)$$

The advantage is that, when written in the Sturmian basis, all the matrix elements representing the various parts of the Floquet Hamiltonian have some strong selection rules. The selection rules on K trivially come from the Fourier expansion of the time dependences; the selection rules on L and M originate from the angular dependence of the various operators. The selection rules on n are far from obvious and are at the heart of the definition and properties of the Sturmian functions [37].

If we define:

$$\begin{aligned} H_0 &= \frac{\mathbf{p}^2}{2} - \frac{1}{r} - i \frac{\partial}{\partial t}, \\ U &= F(x \cos \omega t + \alpha y \sin \omega t), \\ V &= \mathbf{E} \cdot \mathbf{r}, \end{aligned} \quad (2.6)$$

we obtain the following selection rules for the matrices representing these operators in the Sturmian basis [38]:

$$\begin{aligned} \Delta n = 0, \pm 1, \quad \Delta L = 0, \quad \Delta M = 0, \quad \Delta K = 0, & \quad \text{for } H_0 \text{ and unity operators,} \\ \Delta n = 0, \pm 1, \pm 2 \quad \Delta L = \pm 1, \quad \Delta M = 0, \pm 1 \quad \Delta K = 0, & \quad \text{for } V, \\ \Delta n = 0, \pm 1, \pm 2, \quad \Delta L = \pm 1, \quad \Delta M = \pm 1, \quad \Delta K = \pm 1, & \quad \text{for } U. \end{aligned} \quad (2.7)$$

In addition, all matrix elements are known in closed forms and involve only square roots of rational functions of the various quantum numbers. Note that, because of the non orthogonal character of the Sturmian basis, calculating the Floquet quasi-energies requires to solve a generalized eigenvalue problem rather than a standard one. This is the price to pay for getting sparse matrices.

The exact calculation of the quasi-energies is possible only numerically. However, we are interested in the situation where both the static and the microwave fields are weak. Thus, a perturbative expansion is convenient. We will now perform it at the lowest non-vanishing order for each external field. Because, the zeroth order eigenstates are highly degenerate, we have to use degenerate perturbation theory. A convenient formulation is to use an effective Hamiltonian which, at any order of the calculation, has the same spectrum as the initial Hamiltonian, but acts only inside the degenerate hydrogenic manifold. The details of the method are given in [32]. At first order, the calculation is trivial and the effective Hamiltonian $H^{(1)}$ is just the projection of the perturbation onto the manifold we are considering. If P denotes the projector onto the degenerate ($n_0, K = 0$) manifold, it is simply:

$$H^{(1)} = P(U + V)P = PVP \quad (2.8)$$

since U always changes K by one unit. The non-zero matrix elements of $H^{(1)}$ are those of V with $\Delta n = 0$. Thus $H^{(1)}$ is proportional to the static electric field.

The lowest non-vanishing contribution of the microwave field is at second order. It has the following well-known formal expression:

$$H^{(2)} = PUQ \frac{1}{E_0 - H_0} QUP \quad (2.9)$$

where $E_0 = -1/2n_0^2$ is the unperturbed energy of the hydrogenic manifold and $Q = 1 - P$ is the projector onto the subspace complementary to the hydrogenic manifold.

Explicit calculation of $H^{(2)}$ is not straightforward. Indeed, if one expands the $1/(E_0 - H_0)$ onto the eigenstates of H_0 , one obtains a infinite sum over the discrete states and continuum of the atomic spectrum. The trick is to use the non-orthogonal Sturmian basis defined above. Indeed, the projector P has the following simple expression in this basis:

$$P = \sum_{L,M} |n_0, L, M, 0\rangle \langle n_0, L, M, 0| \frac{1}{2r}, \quad (2.10)$$

and consequently

$$Q = \sum_{L,M,(n,K) \neq (n_0,0)} |n, L, M, K\rangle \langle n, L, M, K| \frac{1}{2r}. \quad (2.11)$$

The last step is to calculate the matrix element of the $1/(E_0 - H_0)$ operator in the Sturmian basis. It is simply accomplished by noting that the operator $(E_0 - H_0)$ is diagonal in L, M and K and tridiagonal in n (i.e. connects only state n to states $n - 1, n$ and $n + 1$). Thus the matrix elements of $1/(E_0 - H_0)$ are simply obtained by solving a triadiagonal set of coupled equations in each (L, M, K) subspace coupled to the initial state.

Finally the whole effective quantum Hamiltonian inside the n_0 -manifold reads

$$H_{\text{eff}} = H^{(1)} + H^{(2)}. \quad (2.12)$$

This Hamiltonian takes into account the *direct* coupling between the levels due to the presence of the static electric field (the term proportional to E) and the *indirect* coupling through all levels of other manifolds, i.e. process of absorption and emission of microwave photons (the term proportional to F^2) [32]. Because of the selection rules on the U and V operators and the simple algebraic structure of the effective Hamiltonian, H_{eff} itself has the following selections rules: $\Delta n = 0, \Delta K = 0$ (by construction) and $\Delta L = 0, \pm 1, \pm 2, \Delta M = 0, \pm 1, \pm 2$. The diagonalization of H_{eff} , i.e. of the sparse banded matrix of dimension n_0^2 , by standard routines, yields quasienergies of the system.

The method has been tested in limiting situations, e.g., for parallel weak static and linearly polarized fields where quasienergies resulting from the effective Hamiltonian could be compared with exact diagonalization values. The results for EP presented below are obtained for field amplitudes for which excellent agreement between exact and perturbative results have been found in the limiting cases.

B. Semiclassical perturbation method

The general prescription for the semiclassical quantization of a time-periodic system has been described in [39]. Recently, we used a similar procedure for a LP microwave [40], for a static electric field parallel to a LP microwave [41] and for a two-dimensional model atom in the EP microwave case [24,25].

The method requires first to define a classical Hamilton function for which one can use the usual semiclassical quantization rules. This is done by passing to the extended phase space, defining the momentum p_t conjugate to the t (time) variable. It yields the new classical Hamiltonian, $\mathcal{H}_{\text{Floquet}} = H + p_t$ [26], being the classical analog of the quantum Floquet Hamiltonian, Eq. (2.2).

As the next step, we express the Hamiltonian in action-angle variables of the unperturbed Coulomb problem [42,43]. Due to its high symmetry, several choices are possible. The standard solution is to consider the canonically conjugate pairs (J, Θ) , (L, Ψ) and (M, Φ) . J is the principal action (corresponding to the principal quantum number), i.e. the total action along an unperturbed Kepler elliptical trajectory of the electron. It is simply related to the size of the ellipse. The corresponding angle, Θ , determines the position of the electron on its elliptical trajectory and depends linearly on time, $\Theta \sim \omega_K t$, for an unperturbed atom. L is the angular momentum, Ψ the angle of rotation around the axis defined by the angular momentum vector. Similarly, M, Φ denote the projection of the angular momentum on the laboratory z -axis and the angle of rotation around that axis, respectively. The shape of the ellipse is best described by its eccentricity $e = \sqrt{1 - L^2/J^2}$ while its orientation in the configuration space is determined by the Euler angles $(\Phi, \arccos M/L, \Psi)$ as defined by Goldstein [44].

Using these canonical coordinates, it is possible to write down the full Floquet Hamiltonian. We now specialize to the resonant case where the microwave frequency is an integer multiple of the Kepler frequency of the unperturbed electron, i.e. $\omega_0 = \omega/\omega_K = m$. The corresponding action is:

$$J = n_0 = \omega_K^{-1/3} = \left(\frac{\omega}{m}\right)^{-1/3}. \quad (2.13)$$

n_0 is interpreted as the principal quantum number of the quantum hydrogenic manifold where the resonance takes place.

In the absence of any external field, the variables (J, L, Ψ, M, Φ) are all constant while Θ evolves linearly in time (see above). Hence, in the presence of weak external fields, the motion along the Θ variable will be much faster than along the other coordinates and the secular perturbation theory [26] can be used: it averages over the nonresonant terms and yields the approximate resonant Hamiltonian of the form

$$\mathcal{H}_{\text{sec}} = -\frac{1}{2n_0^2} - \frac{3m^2}{2n_0^4} \hat{J}^2 + F\Gamma_m \cos(\hat{\Theta} - \delta) + E\gamma + \hat{p}_t \quad (2.14)$$

where

$$\begin{aligned} \gamma = & -\frac{3}{2}n_0^2 \left[\cos \varphi \sin \theta \left(\cos \Phi \cos \Psi - \frac{M}{L} \sin \Phi \sin \Psi \right) \right. \\ & + \sin \varphi \sin \theta \left(\sin \Phi \cos \Psi + \frac{M}{L} \cos \Phi \sin \Psi \right) \\ & \left. + \cos \theta \sqrt{1 - \frac{M^2}{L^2}} \sin \Psi \right] \sqrt{1 - \frac{L^2}{n_0^2}}. \end{aligned} \quad (2.15)$$

and

$$\hat{\Theta} = m\Theta - \omega t, \quad \hat{J} = \frac{J - n_0}{m}, \quad \hat{p}_t = p_t + \frac{\omega J}{m}, \quad (2.16)$$

The secular variables $\hat{\Theta}, \hat{J}, \hat{p}_t$ are slowly varying variables obtained by subtracting the unperturbed resonant quantities. $\hat{\Theta}$ represents the phase drift of the electron along the elliptical orbit and \hat{J} the distance (in action) to the exact resonance.

The orientation of the static field with respect to the z -axis is determined by the usual spherical angles, φ and θ . The expression for γ looks complicated, but it is actually nothing but the component of the average atomic dipole on the static field axis. Similarly, $\Gamma_m(L, \Psi, M, \Phi; \alpha)$ and $\delta(L, \Psi, M, \Phi; \alpha)$ just represent the amplitude and the phase of the atomic dipole at the microwave frequency. They can be obtained simply from the Fourier components of the electron position on an unperturbed elliptical trajectory. The explicit, rather complicated formulae for $\delta(L, \Psi, M, \Phi; \alpha)$ and $\Gamma_m(L, \Psi, M, \Phi; \alpha)$ are given by Eq. (2.15) and Eq. (2.16) of [43], respectively and are reproduced in Appendix A for the convenience of the reader.

The last stage is to quantize the system using the approximate Hamiltonian, Eq. (2.14). As any explicit time dependence has disappeared in the secular Hamiltonian, the quantization of \hat{p}_t is trivial. Taking into account that eigenstates of the Floquet Hamiltonian have to be time-periodic, this yields $\hat{p}_t = k\omega$ (where k is an integer number) [39,40] which ensures the periodicity of the quasienergy spectrum with a period ω .

The radial motion, i.e. in the $(\hat{J}, \hat{\Theta})$ effectively decouples from the secular motion of the elliptical trajectory, i.e. in the (L, Ψ, M, Φ) space [42,45]. While considering the radial motion, the effective hamiltonian for the secular part is approximately constant (for a detailed discussion as well as possible counterexamples in some cases see [42]). In effect the quantization resembles in spirit the Born-Oppenheimer approximation. One may first quantize the radial motion keeping the secular motion frozen. The radial motion exhibits a pendulum-like dynamics whose quantum eigenvalues are given by the solutions of the Mathieu equation (see the similar treatment for one-dimensional systems [46–49]). Hence, we can define an effective Hamiltonian acting in a reduced (L, ψ, M, ϕ) phase space just replacing the $(\hat{J}, \hat{\Theta})$ part of \mathcal{H}_{sec} by the quantized energy levels of the pendulum. In this paper, we are interested in the ground state of the pendulum, thus, the quantization of the radial motion yields the following effective Hamiltonian for the secular motion:

$$\mathcal{H}_{\text{eff}} = -\frac{3m^2}{8n_0^4} a_0(q) + E\gamma, \quad (2.17)$$

where the constant terms $-1/2n_0^2$ and $k\omega$ are omitted (\mathcal{H}_{eff} denotes the shift from the unperturbed energy level of the atom), and:

$$q = \frac{4n_0^4 F}{3m^2} \Gamma_m. \quad (2.18)$$

is a dimensionless parameter. $a_0(q)$ is the Mathieu parameter [50] corresponding to the ground state of the pendulum. We can introduce scaled quantities:

$$F_0 = n_0^4 F \quad (2.19)$$

$$E_0 = n_0^4 E \quad (2.20)$$

$$L_0 = \frac{L}{n_0} \quad (2.21)$$

$$M_0 = \frac{M}{n_0} \quad (2.22)$$

$$\Gamma_{m,0} = \frac{\Gamma_m}{n_0^2} \quad (2.23)$$

$$\gamma_0 = \frac{\gamma}{n_0^2}. \quad (2.24)$$

The effective Hamiltonian is:

$$\mathcal{H}_{\text{eff}} = -\frac{3m^2}{8n_0^4}a_0(q) + \frac{E_0}{n_0^2}\gamma_0. \quad (2.25)$$

For a large microwave field amplitude or in the deep semiclassical limit, i.e. $n_0 \rightarrow \infty$, we may employ the asymptotic expression, for large q , of the Mathieu parameter [50]

$$a_0(q) \rightarrow -2q + 2\sqrt{q}. \quad (2.26)$$

This corresponds to the case where the pendulum is localized near its stable equilibrium position (whose energy is $-2q$), its zero-point energy in the ground state being calculated in the harmonic approximation (hence the $2\sqrt{q}$ term).

In the opposite limit, i.e. for $q \ll 1$, another approximation exists $a_0(q) \approx -q^2/2$ [50]. This corresponds basically to a very weak trapping pendulum potential, where the motion is basically the free motion only slightly perturbed (at second order in the energy) by the potential. This is the classical counterpart of the quantum perturbative approach developed above, the equivalent of the “no n -mixing” approximation. In the following, we restrict ourselves to this case as more appropriate for moderate n_0 and very small F_0 . Hence, the final expression for the effective secular Hamiltonian we are going to deal with is

$$\mathcal{H}_{\text{eff}} = \frac{F_0^2}{3m^2}\Gamma_{m,0}^2 + \frac{E_0}{n_0^2}\gamma_0. \quad (2.27)$$

This Hamiltonian is a semiclassical counterpart of the quantum effective Hamiltonian, Eq. (2.12), namely first order in the static electric field and second order in the resonant microwave field.

To calculate the quasienergies semiclassically, one should quantize the secular motion determined by the Hamiltonian (2.27). It has been done in simpler situations (e.g. an hydrogen atom perturbed by a linearly polarized microwave field and a parallel static electric field [41]). Then, the secular motion is integrable and its quantization straightforward using the WKB quantization rule. The present secular problem has two degrees of freedom and turns out to be non-integrable except for some limiting cases. Therefore, a detailed analysis of the classical motion in the phase space of secular variables is necessary for possible comparison with quantal data.

III. PURE MICROWAVE PERTURBATION CASE

Let us consider first the perturbation of an hydrogen atom by an elliptically polarized microwave field in the absence of the static field. Our previous studies of resonant driving of

the atom were restricted to the simplified two-dimensional model atom where the electronic motion is restricted to the polarization plane [24,25]. Then, the classical secular motion is one-dimensional and application of the WKB quantization rule gives very accurate results for quasienergies of the system. In a realistic three-dimensional model, a similar procedure is no longer possible as the effective classical Hamiltonian for a general EP field is not integrable. The secular motion of the atom for weak microwaves, see Eq. (2.27), is determined by the Hamiltonian

$$\mathcal{H}_{\text{eff}} = \frac{F_0^2}{3m^2} \Gamma_{m,0}^2(L_0, \Psi, M_0, \Phi; \alpha). \quad (3.1)$$

The integrable motion is obtained in the limiting polarization cases, i.e. $\alpha = 0$ or 1 , only. That is, for the LP field, the angular momentum projection on the polarization axis is a constant of motion. For the CP case, because of circular symmetry of the field, Φ becomes a cyclic variable and the secular motion is also effectively one-dimensional. Clearly, for α close to these limiting values, the secular motion will be close to integrable. With this in mind, looking for chaotic dynamics, we take $\alpha = 0.4$ in the following (we have verified that this value is representative for a typical EP behaviour).

Eq. (3.1) shows that the structure of the classical phase space of the secular motion depends only on the value of $\mathcal{H}_{\text{eff}}/F_0^2$ (beside the integer m labeling the primary resonance). In other words, if the secular motion is non-integrable for some finite field amplitude, it remains non-integrable even for infinitesimally small amplitude. This clearly demonstrates the inapplicability of the Kolmogorov-Arnold-Moser theorem to the highly degenerate Coulomb problem. On the other hand, the time scale of precession of an electronic ellipse is affected by the strength of the perturbation; for very small F_0 , it will be extremely slow, but the trajectories of the secular motion do not depend on F_0 .

Consider the principal 1:1 resonance case, i.e. $m = 1$. To focus on the phase space structure, we have plotted Poincaré surfaces of section (SOS) for a few values of $\mathcal{H}_{\text{eff}}/F_0^2$ in Fig. 1. For high values of the secular energy, the motion is generally regular. However, for an energy interval around $\mathcal{H}_{\text{eff}}/F_0^2 = 0.3$, the mixed character of the motion is apparent, a quite large chaotic layer is clearly visible.

Switching to the 2:1 resonance case (right hand side of Fig. 1) we find, as previously, regular phase space structures for high energy and mixed character of the motion for lower energies. By visual inspection, the secular motion for 2 : 1 resonance looks “more chaotic” with smaller regular islands embedded in a pronounced chaotic layer. Although we have searched quite extensively, we could not find values of α and the energy corresponding to fully chaotic motion. Always at best tiny regular islands have been found.

The mixed character of the secular motion should have consequences on the statistical properties of the quasienergy spectrum inside the n_0 manifold. As the system possesses anti-unitary symmetry invariance, i.e. is invariant under time-reversal combined with the $y \rightarrow -y$ transformation, see Eq. (2.1), the statistical properties are expected to reflect intermediate behavior between the Poisson and GOE character. To calculate the quasienergy spectrum, we employ the quantum effective Hamiltonian Eq. (2.12). One should take care of discrete symmetries of the system. That is, the system is invariant under the $z \rightarrow -z$ transformation as well as the parity combined with translation in time by π/ω transformations. Thus, the whole spectrum of the n_0 -manifold splits into four independent smaller spectra which are unfolded independently in order to study level statistics.

The dynamics of the levels belonging to the $n_0 = 20$ manifold as a function of the polarization degree α , are shown in Fig. 2, for the 1:1 and 2:1 resonance cases. In each panel, for clarity, there is only one of the four independent sub-spectra plotted. Qualitatively, the level dynamics reflects the character of classical motion, i.e. for high energies, one cannot see level repulsion and there are apparently level crossing (actually small avoided crossings). At lower energy, the level dynamics is more irregular with plenty of avoided crossings, a clear signature of classical chaos in the system, compare Fig. 3 which shows this region in more detail.

To make the comparison more quantitative, we have calculated the cumulative nearest neighbor spacing (NNS) distributions, taking levels in the energy intervals $\mathcal{H}_{\text{eff}}/F_0^2 \in [0.02 - 0.045]$ and $[0.00035 - 0.0018]$ for the 1:1 and 2:1 resonance cases, respectively. The intervals have been chosen to correspond to chaotic behavior as much as possible. Fig. 4 presents the results for the 1:1 resonance for principal quantum number n_0 around 55 and for about twice bigger n_0 , i.e. around 100. The similar results corresponding to the 2:1 resonance are plotted in Fig. 5. In all cases, one can observe that the numerical data are intermediate between the Poisson and GOE statistics. However, the behavior of the 1:1 case is closer to Poisson while the 2:1 one to GOE character, in agreement with the more classically chaotic behaviour in the latter case.

Quantitative measures can be obtained by fitting the data to some theoretical NNS distributions. Quite often, this is being done directly on the histograms for the NNS distributions. Such a procedure is, however, bin size dependent and should be avoided. We prefer to fit the integrated (cumulative) distributions which do not suffer from this ambiguity. There are several possible choices for the theoretical distributions. Berry-Robnik statistics [51] corresponds to a superposition of *independent* Poisson and GOE spectra with relative weight q corresponding to the relative volumes of regular and chaotic parts in the classical phase space. Others possibilities are the phenomenological Brody [52] and Izrailev [53] distributions. The explicit expressions for the distributions used can be found in Appendix B. Although the Berry-Robnik distribution relies on some reasonable theoretical grounds while the two other ones are purely phenomenological, it is commonly accepted that, for not very small effective \hbar , the Brody distribution – or much less known Izrailev one – works better than the Berry-Robnik proposition. The latter works well only in the very deep semiclassical limit (very small effective \hbar) where tunneling between regular and chaotic parts of the phase space is negligible. For lower lying states, the “regular” and “irregular” part of the spectrum interact via tunneling, leading to level repulsion between states in the two groups.

This behaviour is clearly visible in Figs. 4 and 5, (b) and (d). There, the Berry-Robnik distribution predicts much more small spacings than actually observed. On the other hand, except for small spacings we have found that Berry-Robnik statistics fits best in most of the cases, compare Fig. 4 and Fig. 5.

The obtained fitted values of the Berry-Robnik parameter and the parameters for the Brody and Izrailev distributions are given in Table I. While, for the latter cases, the parameters have little physical meaning, as mentioned above, q in the Berry-Robnik distribution should measure the fraction of the chaotic phase space. Qualitatively, the value obtained agrees well with classical SOS plots.

We have also studied the spectral rigidity, i.e. the Δ_3 statistics [2,3,6], in order to obtain some information on the long range correlations in the spectra of our system. Spectral

rigidity gives an independent information about the relative measure of the chaotic part of the classical phase space. For a superposition of independent Poisson and GOE spectra, one obtains [54]

$$\Delta_3 = \Delta_3^{Poisson}((1-q)L) + \Delta_3^{GOE}(qL). \quad (3.2)$$

We have fitted our numerical results with this distribution. The results are plotted in Fig. 6 while values of the fitted parameter are put in Table I. It is well known that, at large L , the spectral rigidity deviates from any universal behaviour and saturates. This is a non-semiclassical effect which should take place for larger and larger L as the effective \hbar goes to zero. To fit the parameter q , we have taken into account only data up to $L = 10$ in order not to enter the saturation regions visible in Fig. 6.

Comparing the Poincaré SOS, NNS distributions and Δ_3 statistics of the calculated data, the qualitative agreement between the classical dynamics and the corresponding quantum statistical properties is apparent. The fitted values for the relative measure of the chaotic part of the phase space coming either from the NNS or the Δ_3 distributions agree perfectly and match well the visual aspect of the SOS.

The NNS distributions change a little when the principal quantum number is modified. The $n_0 \approx 55$ case reveals slightly stronger level repulsion (and, therefore, a “more chaotic” character) than the $n_0 \approx 100$ case. This suggests that some tiny regular structures in the classical phase space are not resolved for $n_0 = 55$ but are for $n_0 = 100$. The long range correlations are more dramatically sensitive to n_0 . The saturation of Δ_3 starts at about twice larger distance in L for the higher n_0 value, see Fig. 6. This is in agreement with the theory of Berry [55] where the critical L value scales as $1/\hbar$ (the effective Planck constant in our problem is $1/n_0$). For large L , the Δ_3 statistics saturates at almost twice bigger value for $n_0 \approx 100$ than $n_0 \approx 55$ again in a qualitative agreement with theory. The latter [55] predicts ($\Delta_3(\infty) \sim 1/\hbar$) for a regular spectrum and ($\Delta_3(\infty) \sim \ln(1/\hbar)$) for a strongly chaotic system. We deal with an intermediate system with mixed phase space, thus we expect the numerical $\Delta_3(\infty)$ value to lie in between the two limits. This is indeed the case.

Finally, let us briefly argue what happens for larger microwave field amplitudes. The secular motion, in the weak field limit, is determined by the effective Hamiltonian, Eq. (3.1), which in turn is a function of $\Gamma_{m,0}$. Increasing the field amplitude one leaves the validity range of the Eq. (3.1) and enters the region where Eq. (2.26) is applicable. Then the orbital electronic motion becomes localized inside a resonance island. The secular motion, however, remains unchanged because the new effective Hamiltonian is again a function of $\Gamma_{m,0}$ only. This means that the spectral statistical properties for higher field amplitude (of course not so big as to produce strong intermanifold mixing) will be the same as the ones presented here. For the high secular energy the motion will be also regular. Thus, one may expect that the nonspreading wavepackets predicted using the two-dimensional model [24,25] will also exist in the real three-dimensional world.

IV. MICROWAVE PLUS STATIC ELECTRIC FIELD

In this section, we discuss the intramanifold behaviour of the hydrogen atom exposed to a resonant microwave field and a static electric field of arbitrary mutual orientation.

For small field amplitudes, the effective secular Hamiltonian is given by Eq. (2.27). The Hamiltonian is the sum of two terms – the first one proportional to F_0^2 (square of the scaled microwave field), the second one to E_0 (scaled static field). For arbitrary mutual orientations of the two fields, the two terms have incompatible symmetry properties and, when having comparable magnitudes, induce a globally chaotic behavior.

Eq. (2.27) has some well defined scaling properties with the field strengths F_0 and E_0 . Let us define the reduced microwave strength

$$\mathcal{F} = F_0^2 n_0^2 / E_0 = F^2 n_0^6 / E \quad (4.1)$$

and the reduced Hamiltonian

$$\mathcal{H} = \mathcal{H}_{\text{eff}} n_0^2 / E_0 = \frac{\mathcal{F}}{3m^2} \Gamma_{m,0}^2 + \gamma_0. \quad (4.2)$$

The classical phase space structure depends only on the value of \mathcal{H} and \mathcal{F} (beside the static field vector orientation and the polarization of the microwave field), but not on the detailed values of n_0 , E_0 , F_0 and the secular energy. Of course, weaker fields imply a slower secular motion, but this does not affect the structure of the phase space. In the quantum mechanical picture, the energy splitting of a degenerate hydrogenic manifold also depends on absolute values of the fields, but the structure of the levels does not.

The application of the static electric field allows us to break any anti-unitary symmetry of the system. It is only for $E_x = 0$ (i.e. $\varphi = \pi/2$) or $E_y = 0$ (i.e. $\varphi = 0$) that the system has some anti-unitary invariance, under the combination of the time-reversal transformation with reflection with respect to the yz or xz plane, see Eq. (2.1).

In a previous letter [31], we have considered the system in the case of the 2:1 resonance driving, i.e. when the microwave frequency is twice the Kepler frequency. Let us consider here first the principal 1:1 resonance, i.e. $m = 1$. A possible signature of the anti-unitary symmetry breaking would be to observe level repulsion with stronger than linear repulsion (i.e. with $P(s) \propto s^\beta$ with $\beta > 1$ for small s). Clearly, it is desirable to have a predominantly chaotic classical dynamics, as a transition from GOE to GUE statistics is expected. To this end, we have to find values of the fields parameters which maximize chaoticity of the system. After rather extensive searches, we have found that $\alpha = 0.4$, $\mathcal{F} = 10$ and $\theta = \pi/4$ are a good choice for that purpose. The remaining spherical angle φ determining the orientation of the static electric field vector, is used to control the breaking of the anti-unitary symmetry.

In Fig. 7, we show Poincaré SOS for a few values of \mathcal{H} , for two cases: $\varphi = 0$ and $\pi/2$. One can see that, for $\varphi \approx \pi/2$, a predominantly chaotic structure space exists in phase space for a large range of secular energies. For $\varphi = \pi/2$, the generalized time reversal invariance holds, as mentioned above. Thus, to study the symmetry breaking, it is interesting to e.g. decrease (or increase) φ gradually, collecting quantum data for some φ values. Note that the addition of the static field tends to make the classical dynamics slightly more chaotic, compare Figs 1 and 7.

The data are then analyzed as in the previous Section – an example is shown in Fig. 8 for two different orientations of the electric field $\varphi = \{0.4\pi, \pi/2\}$. For each φ , data have been collected for principal quantum number n_0 in the range 50-59. Then, we have chosen levels from the scaled energy interval $\mathcal{H} \in (0, 1.4)$, unfolded each spectrum and calculated NNS distributions and spectral rigidities. The cumulative NNS distributions are plotted in

Fig. 8. One can see that the NNS distribution corresponding to the anti-unitary invariant case, $\varphi = \pi/2$, is close to, but does not reach completely the GOE behavior. Similarly, for the $\varphi = 0.4\pi$ case, the distribution is very close, but does not reach the GUE one. Nevertheless, the symmetry breaking is apparent and the numerical spectrum at $\varphi = 0.4\pi$ shows much more level repulsion than the GOE case, which is a clear-cut signature of the breaking of any anti-unitary symmetry.

To measure departures from the entirely ergodic behavior, we can also use the Berry-Robnik distribution. The Berry-Robnik model for fully broken antiunitary symmetry consists of the superposition of two independent Poisson and GUE spectra. The results of the fits are collected in Table II. We have not applied the Brody distribution to the broken anti-unitary invariance case, as the distribution is defined only for Brody parameter less than unity, and does not make any sense in the unitary case. The Izrailev distribution does not suffer this severe problem, and contain all limiting cases ($\beta = 0$ for Poisson statistics, $\beta = 1$ for GOE and $\beta = 2$ for GUE). We have thus fitted our results with this distribution too.

In all cases, the Izrailev distribution works much better than the Berry-Robnik ansatz, presumably because chaotic motion occupies most of the phase space and regular regions are very tiny as seen from Fig. 7 and from the values of q obtained.

The values of the fitted Berry-Robnik parameter are consistent with the character of the corresponding classical motion. An independent information about the relative measure of a chaotic part of phase space comes from the fit of the Δ_3 statistics, Fig. 9 [for broken anti-unitary invariance case Δ_3^{GOE} is substituted by Δ_3^{GUE} in Eq. (3.2)], which turns out to agree very nicely with the values of the Berry-Robnik parameter.

By gradually decreasing φ , we may observe the *partial* symmetry breaking by studying the variation of fitted parameters with φ . Such a transition has been analytically studied for gaussian random matrices [56,57] where the two-point correlation function was analytically found for an appropriate ensemble which interpolated between the GOE and the GUE. A further link with the dynamics of fully chaotic systems with partially broken antiunitary symmetry was also established [58]. These developments cannot be used here since the dynamics in our case is not fully chaotic (as seen from SOS plots and the non-integer level repulsion β parameters for extreme cases of preserved and broken antiunitary symmetry, see Table II).

On the other hand, the Izrailev distribution is quite suitable since it should be a reasonable approximation both for a partial symmetry breaking and a mixed dynamics (it would be possible to construct an analog of Berry-Robnik distribution for such a case but it would be of little practical importance).

Fig. 10 summarizes the changes of the fitted Izrailev parameter β (small s repulsion) with φ . For $\varphi = \pi/2$, it is minimal and equal to 0.85 (see also Table II) for n_0 around 55. With departure from the value $\varphi = \pi/2$ where the anti-unitary symmetry exists, it rapidly increases (filled circles) up to the maximal value 1.73 for $\varphi = 0.4\pi, 0.6\pi$. For still lower (higher) values of φ , the trend is reversed and β starts to decrease. This, at first glance, is a surprising effect (since the symmetry should not yet start to restore). However, it is most probably due the fact that the classical motion becomes more regular as φ is far from $\pi/2$. Observe in Fig. 7 that the SOS around $\varphi = 0$ is much more regular than for $\varphi = \pi/2$.

In order to test this hypothesis, we have used another n_0 value. Indeed, if the dip of β

near $\varphi = \pi/2$ was due to classical reasons, it should not depend on \hbar , i.e. n_0 . Fig. 10 shows also the fitted β parameters for n_0 around 100. Generally, the β values obtained are slightly larger than for lower n_0 . Clearly, φ starts to decrease again around the value $\varphi = 0.4\pi$. On the other hand, the dip of β when φ goes to $\pi/2$ (where an anti-unitary symmetry exists) is faster than for lower n_0 . This is in a full qualitative agreement with RMT [5,6]: for the GOE \rightarrow GUE transition the parameter controlling the transition is proportional to $N^{-1/2}$ where N is the matrix dimension. The size of our matrices scales as n_0^2 , so the parameter controlling the breaking (i.e. a deviation from $\pi/2$ value) should scale like $n_0^{-1} \propto \hbar_{\text{eff}}$. Such a behaviour is roughly observed in Fig.10.

Fig. 11 shows the “maximal” repulsion case obtained, i.e. data for n_0 around 100 and $\varphi = 0.4\pi$. The numerical data are presented in the form of the histogram of spacings and compared with the Izrailev distribution (the fit has been performed, as usual, for the cumulative distribution; the resulting $\beta = 1.83$ value has been used to plot the Izrailev distribution). The dash-dotted and dashed curves correspond to Wigner GOE and GUE distributions, respectively. The fact that we observe level repulsion much stronger than the GOE behaviour is a signature of anti-unitary symmetry breaking.

As mentioned before, our first results on the manifestations of symmetry breaking in our system have been obtained for the microwave frequency being twice the Kepler frequency, i.e. for the 2:1 resonant driving [31]. This choice was motivated by SOS plots in the absence of the electric field - see Fig. 1 - showing smaller regular islands for higher microwave frequency. However, as we have seen above, the presence of the electric field makes the secular motion in the principal resonance island chaotic enough and in fact we get stronger repulsion for the 1 : 1 resonance than for the 2 : 1 situation reported before [31]. For completeness, we show in Table III the fitted parameters obtained from the numerical results reported in [31] using either the spacing distribution or the spectral rigidity Δ_3 . As can be seen, the conclusions we obtain from these results completely confirm the analysis of the 1:1 resonance.

As far as we know, the studied system constitutes the first experimentally realizable example of a quantum system with broken anti-unitary symmetry. We have considered small, but finite, field amplitudes to stay well within the applicability range of the perturbation theory. Nevertheless, this is experimentally feasible: for $n_0 \approx 55$ and $F_0 \approx 5 \times 10^{-4}$, i.e. about 0.3 V/cm, the mean level spacing is of the order of MHz.

For stronger fields, our classical studies also suggest a similar behavior. It could even be that the breaking of the secular approximation makes the system more chaotic and that the statistical properties will be closer to GUE. However, we are not able to show quantum numerical results as they require full quantum numerical treatment which is difficult with the present computer resources and must be left for a future work.

V. CONCLUSIONS

We have considered an hydrogen atom perturbed by a resonant elliptically polarized microwave field with or without an additional static electric field of different orientation, in the limit of small field amplitudes. Classically, such fields may produce chaotic dynamics in the secular motion of the electronic elliptical trajectory. In quantum mechanical language, states coming from a given hydrogenic manifold may be mixed significantly only with each other. Such a situation has been interpreted as a signature of an intramanifold chaos.

For the pure microwave problem, we have studied two different resonant driving cases, i.e. the 1:1 and 2:1 resonances between the microwave field and the unperturbed Kepler motion. Quantizing the fast orbital electronic motion, one can derive an effective Hamiltonian describing the slow secular precession of the electronic elliptical trajectory. For a generic elliptical polarization, the effective Hamiltonian has two degrees of freedom and turns out to be non-integrable. By means of Poincaré surfaces of sections, we have found a range of the secular energy where the phase space reveals mixed character with a significant amount of chaotic layer. Switching to a quantum perturbation calculation, we have shown that the statistical properties of the corresponding quasienergy levels reveal an intermediate behavior between Poisson and GOE character. For the 2:1 resonance case, the classical phase space is significantly more irregular than for the 1:1 case and, consequently, the spectral properties are closer to the GOE behavior.

The application of an additional static electric field to the system has allowed us to enhance chaos in the secular motion. Moreover, the static electric field, for a generic orientation, breaks any anti-unitary symmetry of the system which has a dramatic effect on statistical properties of quasienergy levels. This is the first, to our knowledge, experimentally realizable quantum system, with corresponding chaotic classical behavior, which exhibits breaking of any generalized time-reversal symmetry.

We have studied the principal 1:1 resonance for two slightly different static field orientations: the first one corresponds to the anti-unitary invariance case, the other one to breaking such a symmetry. The classical phase space structures, in both cases, are similar with predominately chaotic behavior. However, the statistical properties of the quantum spectrum change from a near-GOE to a near-GUE behavior when one switches from the preserved to broken anti-unitary symmetry case. In the intermediate situations, we could observe a partial symmetry breaking effect due to the finite size of matrices involved in the problem.

We have studied the limit of small field amplitudes as it allows us to employ quantum perturbation theory. For higher amplitudes, the classical effective Hamiltonian is known, but finding the quasienergy spectrum requires *full* quantum numerical calculations. For a pure microwave perturbation, however, we may predict that statistical properties of the quantum spectrum, for stronger field, should be the same as for weak field limit. This is because of the specific form of the effective Hamiltonian, Eq. (2.17), which depends on dynamical variables only through the Γ_m .

VI. ACKNOWLEDGEMENTS

We are grateful to Felix Izrailev for the permission to use his code for his NNS distribution. We thank the referee for bringing references [56–58] to our attention. Support of KBN under project 2P302B-00915 (KS and JZ) is acknowledged. KS acknowledges support by the Alexander von Humboldt Foundation. The additional support of the bilateral Polonium and PICS programs is appreciated. Laboratoire Kastler Brossel de l’Université Pierre et Marie Curie et de l’Ecole Normale Supérieure is UMR 8552 du CNRS.

VII. APPENDIX A

The amplitude and the phase of the atomic dipole at the microwave frequency, $\Gamma_m(L, \Psi, M, \Phi; \alpha)$ and $\delta(L, \Psi, M, \Phi; \alpha)$ appearing in Eq. (2.14) may be expressed as [43]

$$\Gamma_m = \left\{ \left(\frac{1+\alpha}{2} \right)^2 [V_m^2 + U_m^2] + \left(\frac{1-\alpha}{2} \right)^2 [V_{-m}^2 + U_{-m}^2] + \frac{1-\alpha^2}{2} [(V_m V_{-m} - U_m U_{-m}) \cos 2\Phi - (V_m U_{-m} + U_m V_{-m}) \sin 2\Phi] \right\}^{1/2}, \quad (7.1)$$

and

$$\tan \delta = \frac{(1-\alpha)(V_{-m} \sin \Phi + U_{-m} \cos \Phi) - (1+\alpha)V_m \sin \Phi + U_m \cos \Phi}{(1-\alpha)(V_{-m} \cos \Phi - U_{-m} \sin \Phi) + (1+\alpha)V_m \cos \Phi - U_m \sin \Phi}, \quad (7.2)$$

where V_m and U_m are Fourier expansion terms of the original hamiltonian (2.1) in action-angle variables. Explicitly, they read

$$\begin{aligned} V_0(J, L, \Psi) &= -\frac{3e}{2} J^2 \cos \Psi, \\ U_0(J, L, M, \Psi) &= -\frac{3eM}{2L} J^2 \sin \Psi, \end{aligned} \quad (7.3)$$

and for $m \neq 0$

$$\begin{aligned} V_m(J, L, M, \Psi) &= \frac{J^2}{m} [\mathcal{J}'_m(me) + \frac{M\sqrt{1-e^2}}{Le} \mathcal{J}_m(me)] \cos \Psi, \\ U_m(J, L, M, \Psi) &= \frac{J^2}{m} \left[\frac{M}{L} \mathcal{J}'_m(me) + \frac{\sqrt{1-e^2}}{e} \mathcal{J}_m(me) \right] \sin \Psi. \end{aligned} \quad (7.4)$$

In the above formulae $e = \sqrt{1 - L^2/J^2}$ is an eccentricity of the electronic ellipse while $\mathcal{J}_m(x)$ and $\mathcal{J}'_m(x)$ denote the ordinary Bessel function and its derivative, respectively.

VIII. APPENDIX B

We give here explicit expressions for various level spacing distributions which have been used in the present paper.

The Poisson distribution, corresponding to a system with classically integrable dynamics [7], reads

$$P(s) = \exp(-s). \quad (8.1)$$

For an ergodic classical behavior, the quantum spectrum of a generic system is conjectured [1] to have a nearest neighbor spacing (NNS) distribution (for the unfolded spectrum) similar to that of the random matrices of the same universality class. The resulting NNS distributions are quite complicated (see e.g. [5,6]). However, a good approximation is given by the so called Wigner surmise, obtained for matrices of rank 2. These are:

$$P(s) = \frac{\pi}{2}s \exp\left(-\frac{\pi}{4}s^2\right) \quad (8.2)$$

for an anti-unitary invariant (GOE) system and

$$P(s) = \frac{32}{\pi^2}s^2 \exp\left(-\frac{4}{\pi}s^2\right) \quad (8.3)$$

for broken anti-unitary invariance (GUE).

The phenomenological Brody distribution [52] which interpolates between Poisson and GOE distributions reads

$$P(s) = C(\beta + 1)s^\beta \exp\left(-Cs^{\beta+1}\right) \quad (8.4)$$

with

$$C = \left[\Gamma\left(\frac{\beta + 2}{\beta + 1}\right) \right]^{\beta+1}, \quad (8.5)$$

$\beta = 0$ (resp. $\beta = 1$) corresponds to the extreme case of the Poisson (resp. GOE) statistics.

Another attempt towards a simple distribution interpolating between different ensembles, is due to Izrailev [53,59] and reads

$$P(s) = As^\beta(1 + sB\beta)^{f(\beta)} \exp\left[\frac{-\pi^2\beta s^2}{16} - \frac{\pi}{4}(2 - \beta)s\right] \quad (8.6)$$

where

$$f(\beta) = \frac{2^\beta(1 - \beta/2)}{\beta} - 0.16874, \quad (8.7)$$

and A, B are constants that ensure

$$\int P(s)ds = 1, \quad (8.8)$$

and

$$\int sP(s)ds = 1. \quad (8.9)$$

It is claimed to work reasonably well for all possible intermediate situations.

While there exist several other propositions in the literature, we list only the so called Berry–Robnik statistics [51]. It may be derived assuming an independent superposition of Poisson spectrum and spectra corresponding to random matrix predictions. If one deals with Poisson and only one GOE spectrum, the Berry–Robnik distribution reads [51]

$$P(s) = \left[2q(1 - q) + \frac{\pi}{2}q^3s\right] \exp\left[(q - 1)s - \frac{\pi}{4}q^2s^2\right] + (1 - q)^2 \exp[(q - 1)s] \operatorname{erfc}\left(\frac{\sqrt{\pi}}{2}qs\right) \quad (8.10)$$

where $0 \leq q \leq 1$ is the relative weight of the GOE spectrum. Classically, q corresponds to the relative volume of the chaotic part of phase space. The similar Berry–Robnik distribution for a superposition of a Poisson spectrum and one GUE spectrum is [60]

$$P(s) = \left\{ \left[\frac{32}{\pi^2} q^4 s^2 + \frac{8}{\pi} q^2 (1-q)s + (1-q)^2 \right] \exp\left(-\frac{4}{\pi} q^2 s^2\right) + \left[2q(1-q) - (1-q)^2 qs \right] \operatorname{erfc}\left(\frac{2}{\sqrt{\pi}} qs\right) \right\} \exp[(q-1)s]. \quad (8.11)$$

Let us present also the expression for the $U(W)$ function which has been employed in a fine-scale representation of the deviation of the numerical level spacing distribution from the best fitting theoretical distribution. The following function [61]

$$U(W) = \arccos \sqrt{1-W}, \quad (8.12)$$

where W is the value of the cumulative level spacing distribution $\int P(s) ds$, ensures that, over the whole range of W , i.e. from 0 to 1, the standard deviation of numerical data is uniform and equal to $\delta U = 1/(\pi\sqrt{N})$, where N is the total number of spacings.

For completeness, let us finally define the spectral rigidity $\Delta_3(L)$ as an average over the spectral range used in analysis (i.e. over x_0) of

$$\Delta_3(x_0, L) = L^{-1} \min_{A,B} \int_{x_0}^{x_0+L} dx (N(x) - Ax - B)^2, \quad (8.13)$$

where $N(x)$ is the integrated level density (a staircase function).

REFERENCES

- [1] O. Bohigas, M. J. Giannoni, and C. Schmit, Phys. Rev. Lett. **52** (1984), 1.
- [2] M. L. Mehta, *Random Matrices* Academic Press, San Diego, 1991.
- [3] T. A. Brody *et al.*, Rev. Mod. Phys. **53** (1981), 385.
- [4] J. Zakrzewski, K. Dupret, and D. Delande, Phys. Rev. Lett. **74** (1995), 522.
- [5] F. Haake, *Quantum Signatures of Chaos*, Vol. 54 of *Springer Series in Synergetics* Springer, Berlin, 1991.
- [6] O. Bohigas, in *Chaos and Quantum Physics, 1989 Les Houches Lecture Session LII*, p.87 (M. J. Giannoni, A. Voros, and J. Zinn-Justin Eds.) North-Holland, Amsterdam, 1991.
- [7] M. V. Berry and M. Tabor, Proc. R. Soc. Lond. A **356** (1977), 375.
- [8] T. Zimmermann *et al.*, Phys. Rev. Lett. **61** (1988), 3.
- [9] P. So, S. M. Anlage, E. Ott, and R. N. Oerter, Phys. Rev. Lett. **74** (1995), 2662.
- [10] U. Stoffregen *et al.*, Phys. Rev. Lett. **74** (1995), 2666.
- [11] J. E. Bayfield and P. M. Koch, Phys. Rev. Lett. **33** (1974), 258.
- [12] J. G. Leopold and I. C. Percival, Phys. Rev. Lett. **41** (1978), 944.
- [13] G. Casati, B. V. Chirikov, D. L. Shepelyansky, and I. Guarneri, Phys. Rep. **154** (1987), 77.
- [14] G. Casati, I. Guarneri, and D. L. Shepelyansky, IEEE J. Quantum Electron. **24** (1988), 1420.
- [15] P. M. Koch, in *Chaos and Quantum Chaos*, Vol. 411 of *Lecture Notes in Physics*, (W. D. Heiss Ed.) Springer, Berlin, 1992.
- [16] P. M. Koch and K. A. H. van Leeuwen, Phys. Rep. **255** (1995), 289.
- [17] R. V. Jensen, S. M. Susskind, and M. M. Sanders, Phys. Rep. **201** (1991), 1.
- [18] M. R. W. Bellermand, P. M. Koch, D. Mariani, and D. Richards, Phys. Rev. Lett. **76** (1996), 892.
- [19] M. R. W. Bellermand, P. M. Koch, and D. Richards, Phys. Rev. Lett. **78** (1997), 3840.
- [20] J. Zakrzewski, R. Gebarowski, and D. Delande, Phys. Rev. A **54** (1996), 691.
- [21] D. Delande and J. Zakrzewski, in *Classical, Semiclassical and Quantum Dynamics in Atoms*, No. 485 in *Lecture Notes in Physics* (H. Friedrich and B. Eckhardt Eds.) p.205 Springer, New York, 1997.
- [22] K. Sacha and J. Zakrzewski, Phys. Rev. **A55** (1997), 568.
- [23] K. Sacha and J. Zakrzewski, Phys. Rev. **A56** (1997), 719.
- [24] K. Sacha and J. Zakrzewski, Phys. Rev. A **58** (1998), 3974.
- [25] K. Sacha and J. Zakrzewski, Phys. Rev. A **59** (1999), 1707.
- [26] A. J. Lichtenberg and M. A. Lieberman, *Regular and Stochastic Motion*, Vol. 38 of *Applied Mathematical Sciences* Springer, Berlin, 1983.
- [27] J. von Milczewski, G.H.F. Dierksen and T. Uzer, Phys. Rev. Lett. **73** (1994), 2428.
- [28] J. von Milczewski and T. Uzer, Phys. Rev. E **55** (1997), 6540.
- [29] J. Main, M. Schwacke, and G. Wunner, Phys. Rev. A **57** (1998), 1149.
- [30] For example, the static electric field used in Fig. 10(a)-(d) of reference [29] or in Fig. 13 of [28] in order to produce a significant chaotic component are so high that the corresponding bound states do not exist any longer, but turn into very broad unresolved resonances.

- [31] K. Sacha, J. Zakrzewski, and D. Delande, Phys. Rev. Lett. **83** (1999), 2922 and **84**, 200 (2000).
- [32] C. C. Cohen-Tannoudji, J. Dupont-Roc, and G. Grynberg, *Atom-Photon Interactions: Basic Processes and Applications* John Wiley and Sons, New York, 1992.
- [33] J. H. Shirley, Phys. Rev. **138** (1965), B979.
- [34] A. Buchleitner, B. Grémaud, and D. Delande, J. Phys. B: Atom. Mol. Opt. Phys. **27** (1994), 2663.
- [35] A. Buchleitner, Ph.D. thesis, Université Pierre et Marie Curie, Paris, 1993, *Atomes de Rydberg en champs micro-onde: régularité et chaos*.
- [36] K. Sacha, Ph.D. thesis, Jagellonian University, Kraków, 1998, *Hydrogen atom in microwave field*, unpublished.
- [37] Equivalently, one can define in the Hilbert space a new scalar product for which the Sturmian basis is orthonormal. The $1/2r$ factor disappears in Eq. (2.5), but all operators have to be multiplied by $2r$ to preserve hermiticity. The choice of one or the other formulation is just a matter of convenience, they are totally equivalent.
- [38] D. Delande, Ph.D. thesis, Université de Paris, Paris, 1988, thèse de doctorat d'état.
- [39] H. P. Breuer and M. Holthaus, Ann. Phys. **211** (1991), 249.
- [40] A. Buchleitner, K. Sacha, D. Delande, and J. Zakrzewski, Eur. Phys. J. D **5** (1999), 145.
- [41] K. Sacha, J. Zakrzewski, and D. Delande, Eur. Phys. J. **D1** (1998), 231.
- [42] J. G. Leopold and D. Richards, J. Phys. B: Atom. Mol. Opt. Phys. **19** (1986), 1125.
- [43] K. Sacha and J. Zakrzewski, Phys. Rev. A **58** (1998), 488.
- [44] H. Goldstein, *Classical Dynamics* p.146 Addison-Wesley, Reading, Ma., 1980.
- [45] J. G. Leopold and D. Richards, J. Phys. B: Atom. Mol. Opt. Phys. **20** (1987), 2369.
- [46] J. Henkel and M. Holthaus, Phys. Rev. **A45** (1992), 1978.
- [47] M. Holthaus, Chaos, Solitons and Fractals **5** (1995), 1143.
- [48] M. E. Flatté and M. Holthaus, Ann. Phys. **245** (1996), 113.
- [49] L. Sirko and P. M. Koch, Appl. Phys. Lett. **B60** (1995), S195.
- [50] in *Handbook of Mathematical Functions*, (M. Abramowitz and I. A. Stegun Eds.) Dover, New York, 1972.
- [51] M. V. Berry and M. Robnik, J. Phys. A **17** (1984), 2413.
- [52] T. A. Brody, Lett. Nuovo Cimento **7** (1973), 482.
- [53] F. M. Izrailev, Phys. Rep. **196** (1990), 299.
- [54] T. H. Seligman and J. J. M. Verbaarschot, J. Phys. A **18**, (1985), 2227.
- [55] M. V. Berry, Proc. R. Soc. Lond. A **400** (1985), 229.
- [56] A. Pandey and M. L. Mehta, Commun. Math. Phys. **87** (1983), 449.
- [57] M. L. Mehta and A. Pandey, J. Phys. A **16** (1983), 2655, L601.
- [58] O. Bohigas, M-J Giannoni, A.M. Ozorio de Almeida, and C. Schmit, Nonlinearity **8** (1995), 203.
- [59] G. Casati, F. M. Izrailev, and L. Molinari, J. Phys. A **24** (1991), 4755 .
- [60] M. Robnik, J. Dobnikar, and T. Prozen, preprint , chaodyn/9711011 (1997).
- [61] T. Prozen and M. Robnik, J. Phys. A **26** (1993), 2371.

TABLES

TABLE I. Fitted parameters for different distributions as defined in the Appendix. The data collected correspond to the hydrogen atom driven by an elliptically polarized microwave field and are shown in Fig. 4 and Fig. 5. For each set of levels, we fit the nearest neighbor spacing distribution or the spectral rigidity Δ_3 and show here the value of the free parameter for the best fit.

	1:1 resonance		2:1 resonance	
	$n_0 = 50 - 59$	$n_0 = 97 - 102$	$n_0 = 50 - 59$	$n_0 = 97 - 102$
q (Berry-Robnik):	0.56	0.47	0.77	0.73
q (Δ_3):	0.55	0.43	0.76	0.73
β (Izrailev):	0.17	0.12	0.42	0.37
β (Brody):	0.23	0.16	0.49	0.44
Time-reversal invariance	Yes	Yes	Yes	Yes

TABLE II. Fitted parameters for different distributions as defined in the Appendix. The data partially shown in Fig. 8 correspond to the hydrogen atom driven by an elliptically polarized microwave field and exposed to an additional static electric field. For each set of levels, we fit the nearest neighbor spacing distribution or the spectral rigidity Δ_3 and show here the value of the free parameter for the best fit.

	$\varphi = 0.4\pi$		$\varphi = \pi/2$	
	$n_0 = 50 - 59$	$n_0 = 97 - 102$	$n_0 = 50 - 59$	$n_0 = 97 - 102$
q (Berry-Robnik):	0.97	0.98	0.95	0.94
q (Δ_3):	0.98	0.98	0.96	0.95
β (Izrailev):	1.73	1.83	0.85	0.82
β (Brody):	–	–	0.85	0.83
Time-reversal invariance	No	No	Yes	Yes

TABLE III. Fitted parameters for different distributions as defined in the Appendix. The data correspond to the 2:1 resonance of the hydrogen atom driven by an elliptically polarized microwave field and exposed to an additional static electric field. For each set of levels, we fit the nearest neighbor spacing distribution or the spectral rigidity Δ_3 and show here the value of the free parameter for the best fit. The data with scaled energy $\mathcal{H} \in (8.5, 9.5)$ and for $\mathcal{F} = 5000$ are analyzed.

	$n_0 = 99 - 101$	$n_0 = 97 - 102$
	$\varphi = 0.2, 0.25, 0.3\pi$	$\varphi = \pi/2$
q (Berry-Robnik):	0.94	0.94
q (Δ_3):	0.94	0.95
β (Izrailev):	1.47	0.82
β (Brody):	–	0.83
Time-reversal invariance	No	Yes

FIGURES

FIG. 1. Poincare surfaces of sections (at $\Phi = 0$) of the classical secular motion, Eq. (3.1), for the hydrogen atom perturbed by a weak resonant microwave field with elliptical polarization (polarization parameter $\alpha = 0.4$). The coordinates used for the plot are the scaled total angular momentum $L_0 = L/n_0$ and its canonically conjugate angle Ψ . Left column – the 1:1 resonance case (microwave frequency equal to the unperturbed Kepler frequency of the electron on its elliptical trajectory) for the secular energies (going from bottom to top), $\mathcal{H}_{\text{eff}}/F_0^2 = 0.02, 0.03, 0.04, 0.07$. Right column – the 2:1 resonance case (microwave frequency is twice the Kepler frequency), for $\mathcal{H}_{\text{eff}}/F_0^2 = 0.0006, 0.0013, 0.0018, 0.0021$ again from bottom to top. Note that, for the parameters chosen, not the whole (L_0, Ψ) space is accessible.

FIG. 2. Energy levels of the $n_0 = 20$ hydrogenic manifold resonantly driven by an elliptically polarized microwave field vs. the degree of polarization, α , for the 1:1 resonance case [panel (a)] and 2:1 resonance case [panel (b)]. We plot the shifts (divided by F_0^2) of the energy levels with respect to the unperturbed energy of the atom. The upper states evolve smoothly with almost exact level crossings, in agreement with the classical mostly regular dynamics. In contrast, most of the lowest states evolve irregularly and sometimes display large avoided crossings, a signature of a classically chaotic behaviour.

FIG. 3. A part of the spectrum of $n_0 = 50$ hydrogenic manifold resonantly driven by an elliptically polarized microwave field vs. the degree of polarization, α , for the 2:1 resonance case in the region of mixed regular and chaotic motion. We plot the shifts (divided by F_0^2) of the energy levels with respect to the unperturbed energy of the atom. Most of the states display large avoided crossings, a signature of a classically chaotic behaviour.

FIG. 4. Cumulative level spacing distribution, $W(s)$, for the pure microwave perturbation (degree of the polarization $\alpha = 0.4$) for the 1:1 resonance case. Levels in the range of $\mathcal{H}_{\text{eff}}/F_0^2 = 0.02 - 0.045$ are analyzed. In panel (a), the solid line represents numerical data for $n_0 = 50 - 59$ (there are about 10000 spacings); the dashed and dash-dotted lines represent the Poisson and GOE distributions respectively. Panel (b) shows a fine-scale representation of the deviation of the numerical level spacing distribution from the best Izrailev distribution in terms of the $U(W) - U(W_{\text{Izrailev}})$ vs. W ; the transformation $U(W) = \arccos \sqrt{1 - W}$ is used in order to have uniform statistical error over the plot - compare [61] and the Appendix. The upper and lower noisy curves represent one standard deviation from the calculated data which lie in the middle of the band. The long-dashed curve represents the best Berry-Robnik distribution while the dotted line the best Brody distribution. Panel (c), the solid line represents the numerical data for $n_0 = 97 - 102$ (there are about 20000 spacings), the dashed and dash-dotted lines represent the Poisson and GOE distributions as in (a). Panel (d) shows the corresponding deviations of the numerical level spacing distribution from the best fits – the notation is the same as in panel (b). Note that the best fitted Berry-Robnik or Izrailev distributions are altogether in excellent agreement with the numerical results. At the scale of (a) and (c), they are not distinguishable from the data.

FIG. 5. The same as in Fig. 4, but for the 2:1 resonance case for the range of $\mathcal{H}_{\text{eff}}/F_0^2 = 0.00035 - 0.0018$.

FIG. 6. Spectral rigidity Δ_3 for the pure microwave perturbation ($\alpha = 0.4$) compared with the random ensemble predictions. Numerical data (solid lines) for $n_0 = 50 - 59$ are shown in panel (a) for the 1:1 resonance case and in panel (b) for the 2:1 resonance. The data for $n_0 = 97 - 102$ are presented in panels (c) and (d) for the 1:1 and 2:1 resonances respectively. The dotted lines are the fits of Eq. (3.2) while the dashed lines indicate the Poisson (upper straight lines) and GOE (lower curves) predictions. Note the saturation at large L , in agreement with the semiclassical prediction.

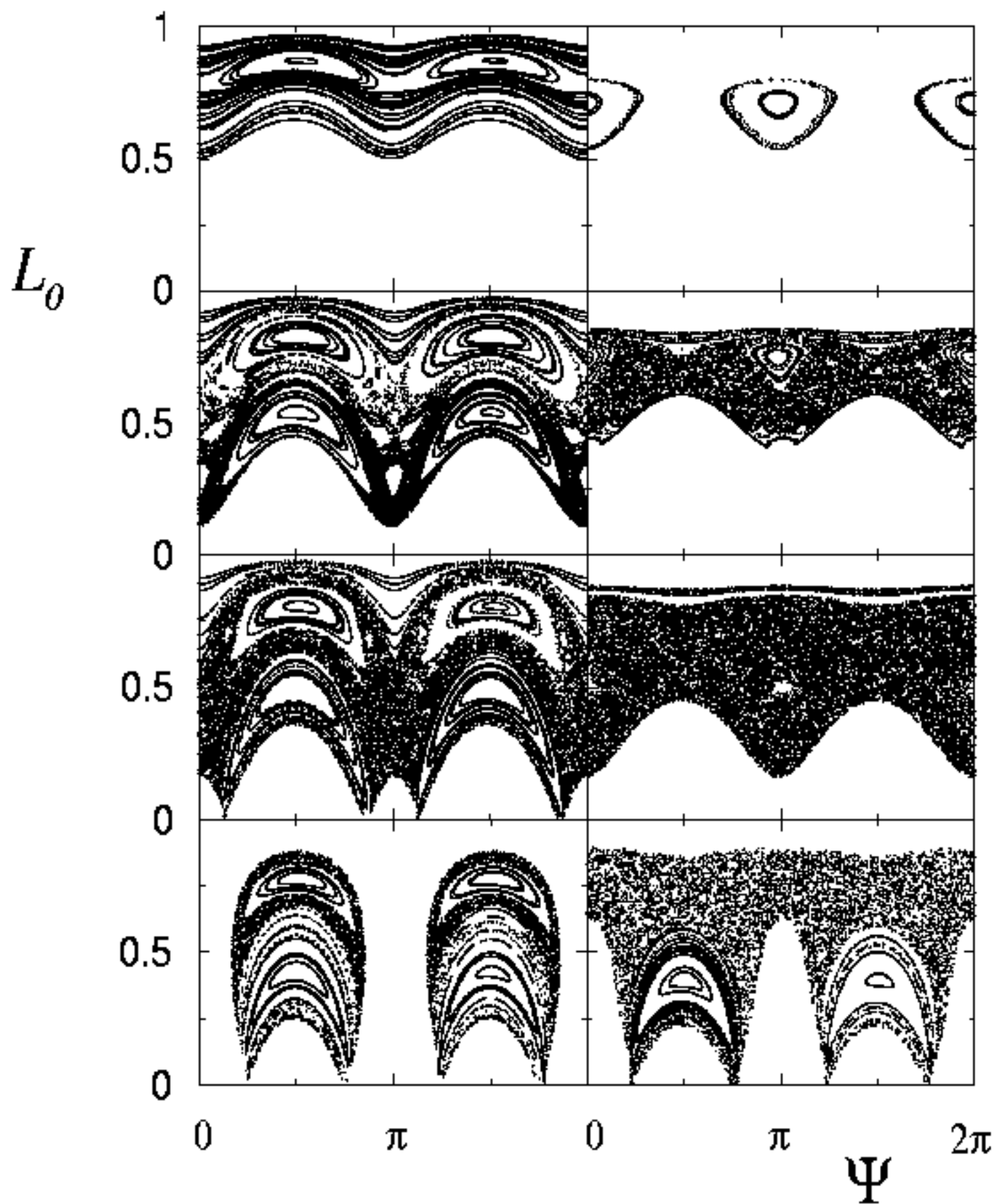
FIG. 7. Poincaré surfaces of section (at $\Phi = 0$) of the classical secular motion, Eq. (4.2), for the hydrogen atom in a static electric field and driven by an elliptically polarized ($\alpha = 0.4$) microwave field resonant with the Kepler frequency (1:1 resonance). Left and right columns correspond to a static electric field with scaled amplitude $\mathcal{F} = 10$ and different orientations $\varphi = 0$, $\theta = \pi/4$ and $\varphi = \pi/2$, $\theta = \pi/4$ respectively. The secular energies (going from bottom to top, the same for left and right panels) are: $\mathcal{H} = -0.2, 0.4, 0.8, 1.4$. Note that, for the parameters chosen, not the whole (L_0, Ψ) space is accessible.

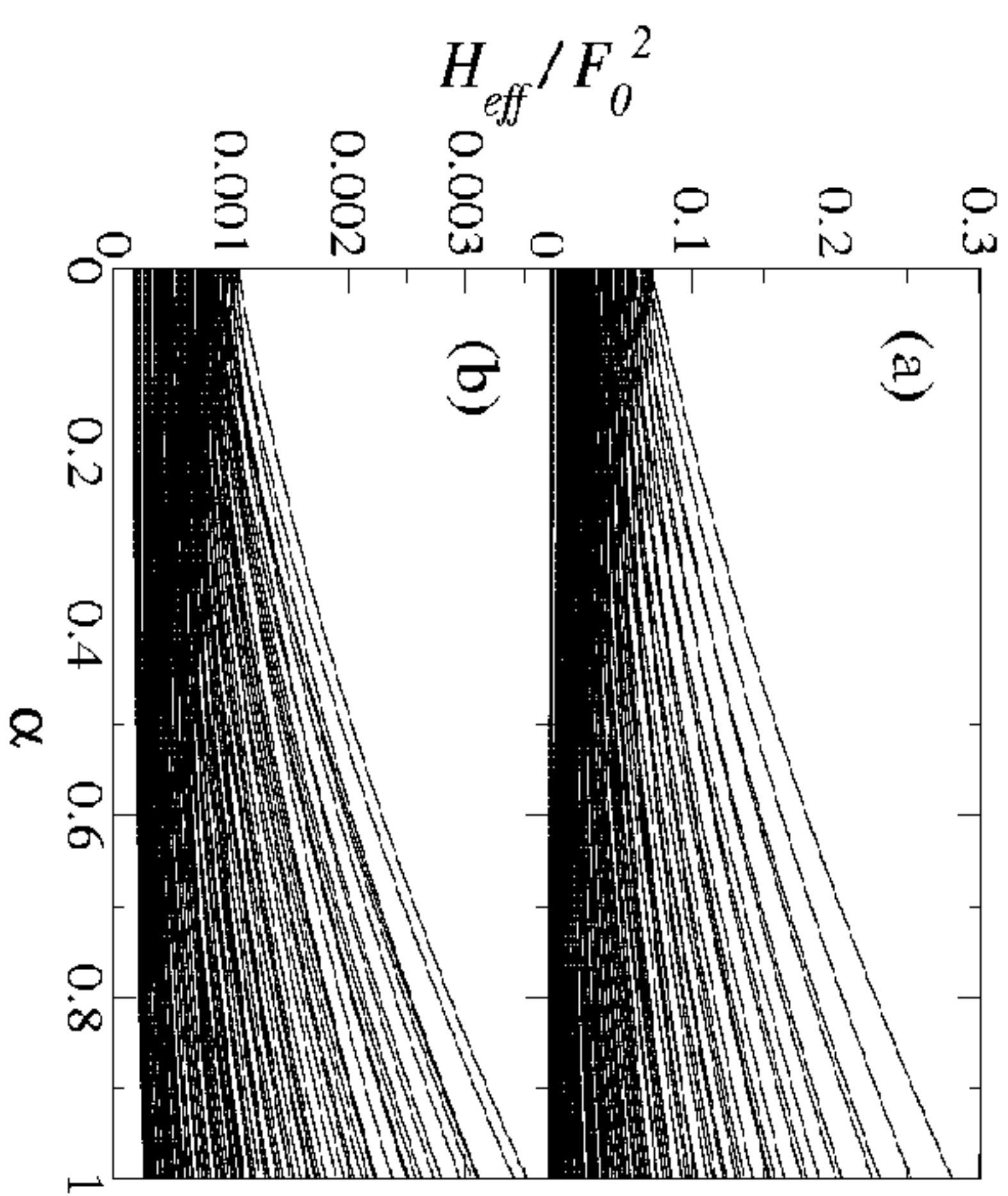
FIG. 8. Cumulative level spacing distribution, $W(s)$, for the the hydrogen atom in an elliptically polarized microwave field (ellipticity parameter $\alpha = 0.4$) combined with a static electric field, for the 1:1 resonance case. Levels in the range of $\mathcal{H} = 0 - 1.4$ and for $n_0 = 50 - 59$ are analyzed (about 20 000 spacings). The value of the reduced microwave strength is chosen as $\mathcal{F} = 10$, while the angle is $\theta = \pi/4$. Panel (a) shows the data (solid line) for $\varphi = 0.4\pi$, i.e. for broken generalized time reversal invariance. The fitted Izrailev distribution cannot be distinguished from numerical data. Dashed and dash-dotted lines correspond to GUE and GOE predictions respectively (thus the data are closer to GUE than GOE). Panel (b) shows the difference between the numerical result and the best Izrailev distribution (horizontal line). The upper and lower noisy curves yield one standard deviation from the numerical data that lie in the middle of the band. The Izrailev distribution stays well within the one standard deviation practically everywhere. The dashed line corresponds to a Berry-Robnik distribution (for the mixture of Poisson and GUE spectra) which is clearly inferior to the Izrailev distribution. Panel (c) and (d) correspond to $\varphi = \pi/2$ where the anti-unitary symmetry is restored. In (c), dashed line corresponds now to Poisson, the data trace the distribution close to GOE one. In panel (d) the dashed-dotted line corresponds to Brody distribution. Clearly Brody and Izrailev distributions practically coincide and work much better than the Berry-Robnik distribution.

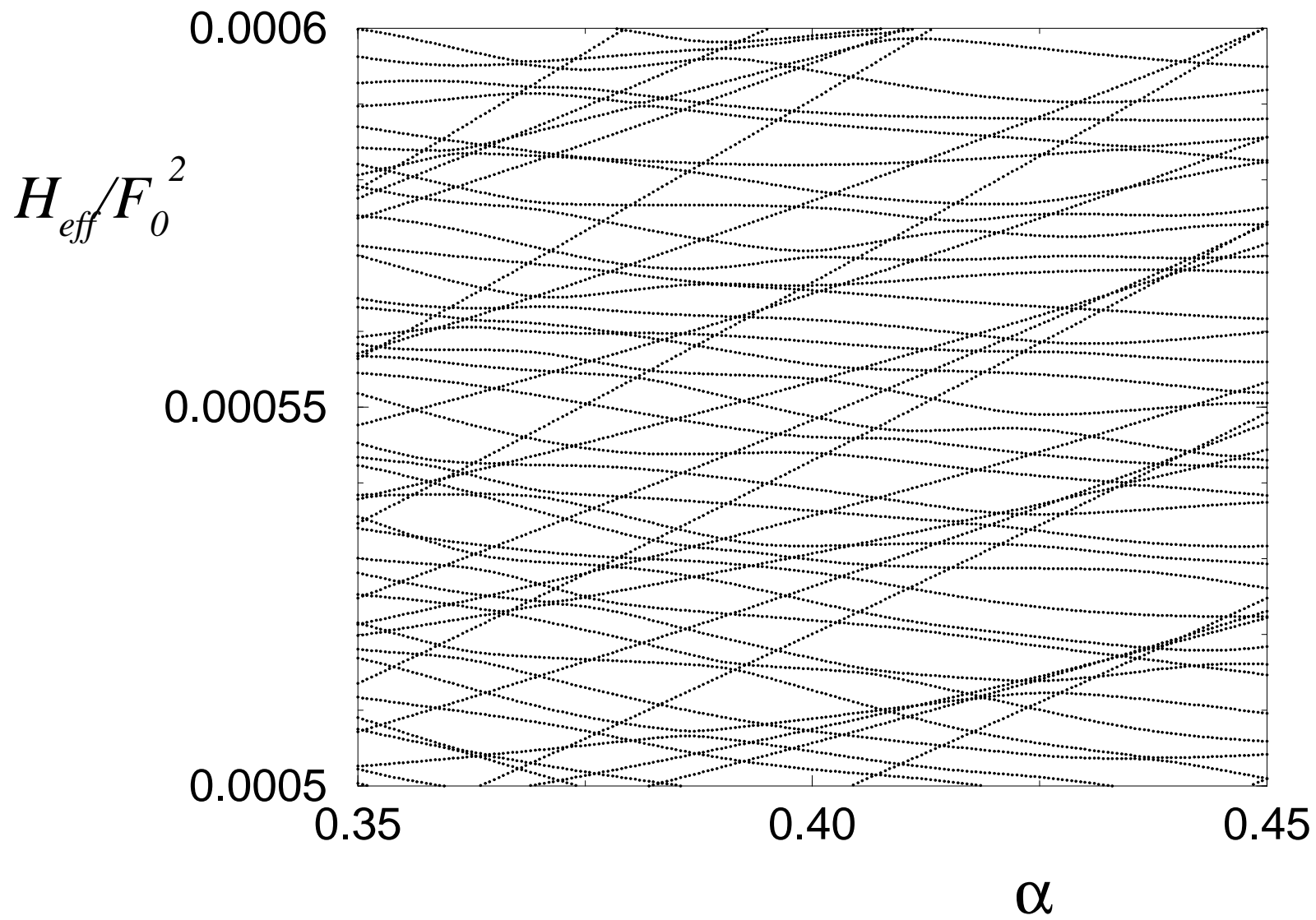
FIG. 9. Spectral rigidity, Δ_3 compared with the random ensemble predictions for the hydrogen atom resonantly driven by an elliptically polarized microwave field in the presence of a static electric field of different orientation. The numerical data used are the same as in figure 8. Panel (a) corresponds to broken anti-unitary symmetry ($\varphi = 0.4\pi$), panel (b) to $\varphi = \pi/2$ (generalized time-reversal invariant case). The dotted lines denote the fit of Eq. (3.2) for (b) and a similar expression for (a) with GUE in place of GOE. The dashed lines indicate the Poisson (upper straight lines), GOE and GUE predictions. Observe that, for broken anti-unitary symmetry, the data trace between the GOE and GUE curves. The typical saturation effects appear for large L .

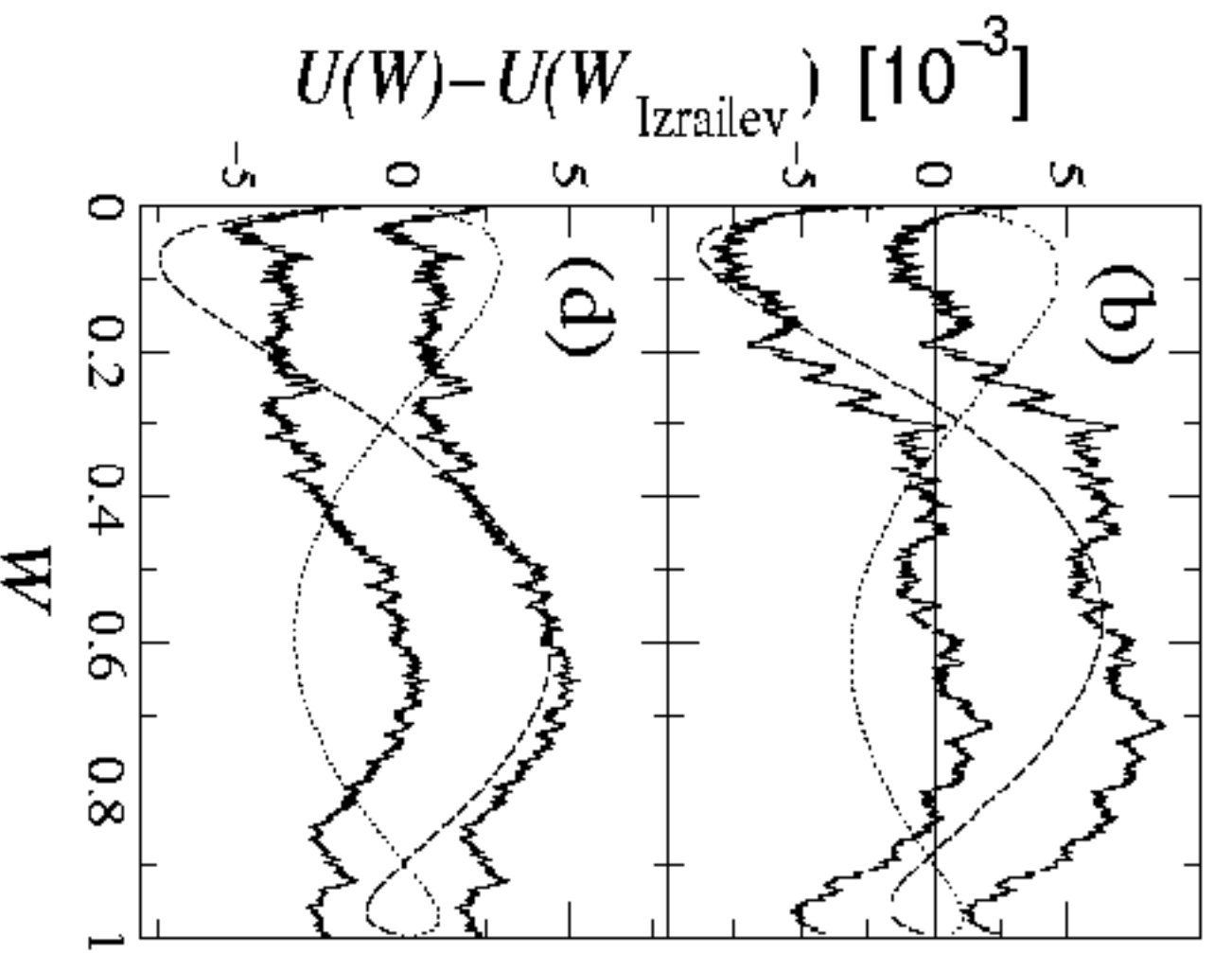
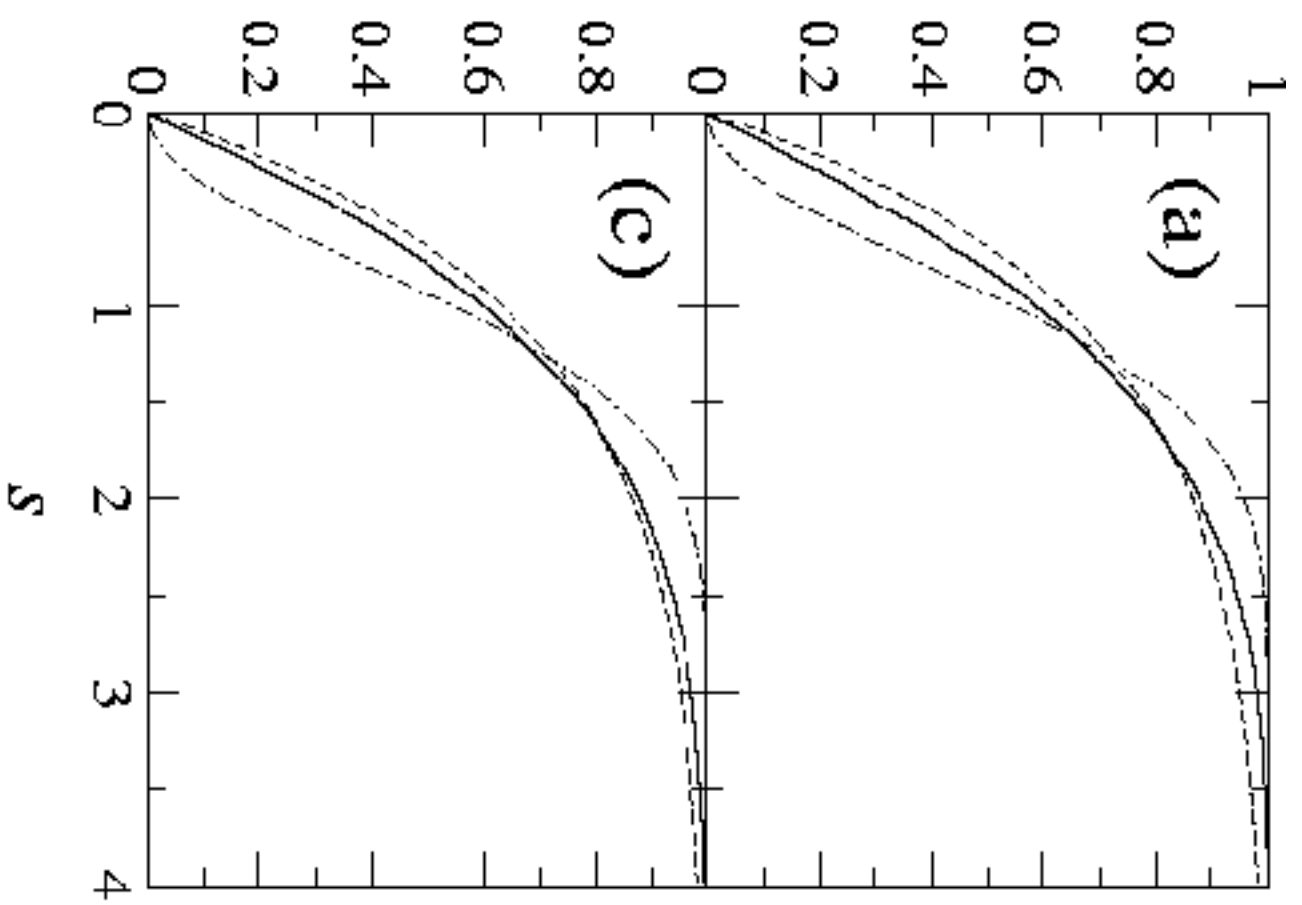
FIG. 10. The gradual symmetry breaking with the orientation of the electric field, i.e. φ . Filled circles correspond to the fitted Izrailev repulsion parameters β for data around $n_0 = 55$, open circles for data around $n_0 = 100$. Close to $\varphi = 0.5\pi$ – where an anti-unitary symmetry exists – there is sudden drop in β by roughly one unit, as predicted by Random Matrix Theory. For smaller (larger – the figure is symmetric around $\pi/2$) values of φ , the classical motion is less chaotic with large regular islands in the phase space – this explains the decrease of β for $\varphi < 0.4\pi (> 0.6\pi)$. For a further discussion, see text.

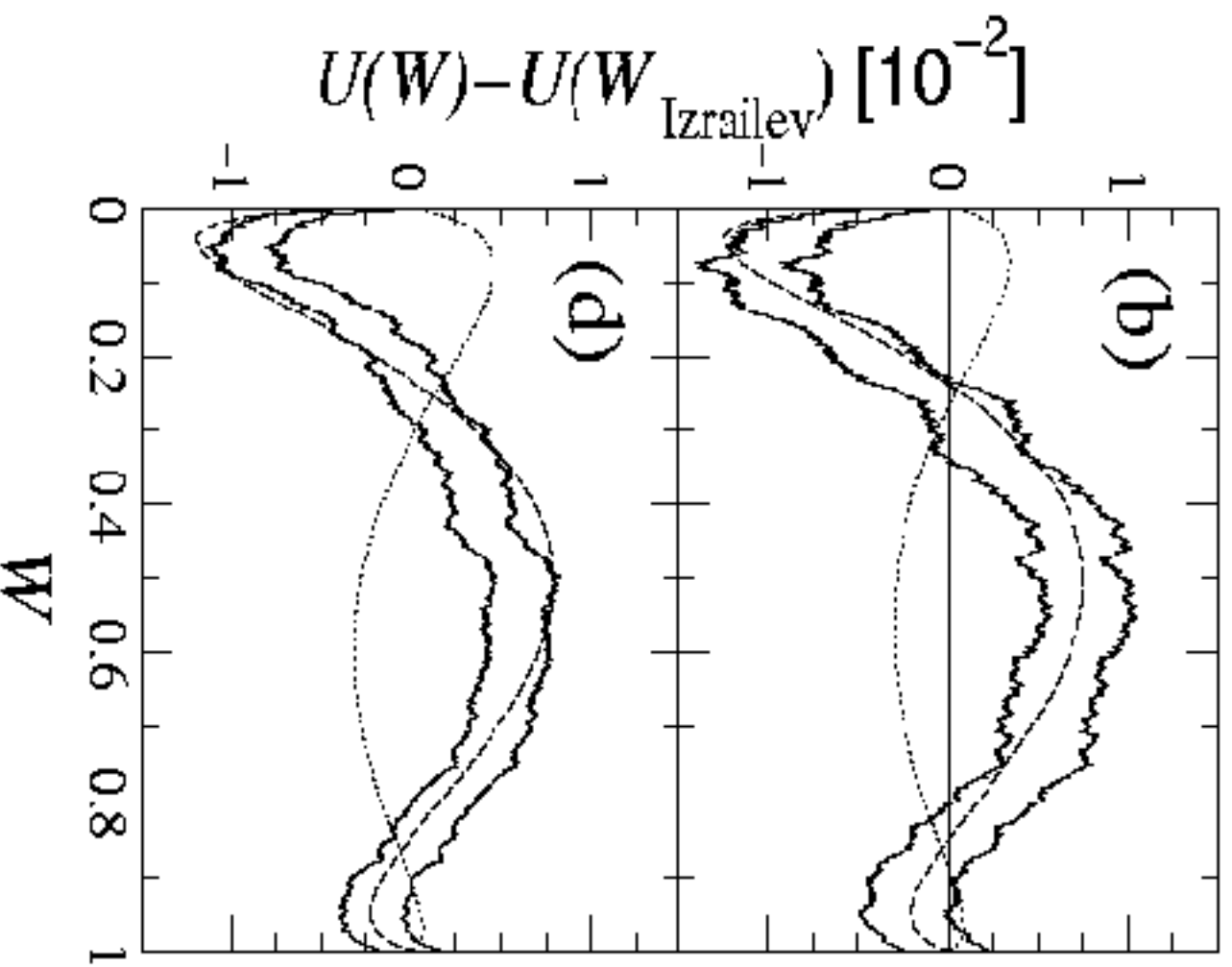
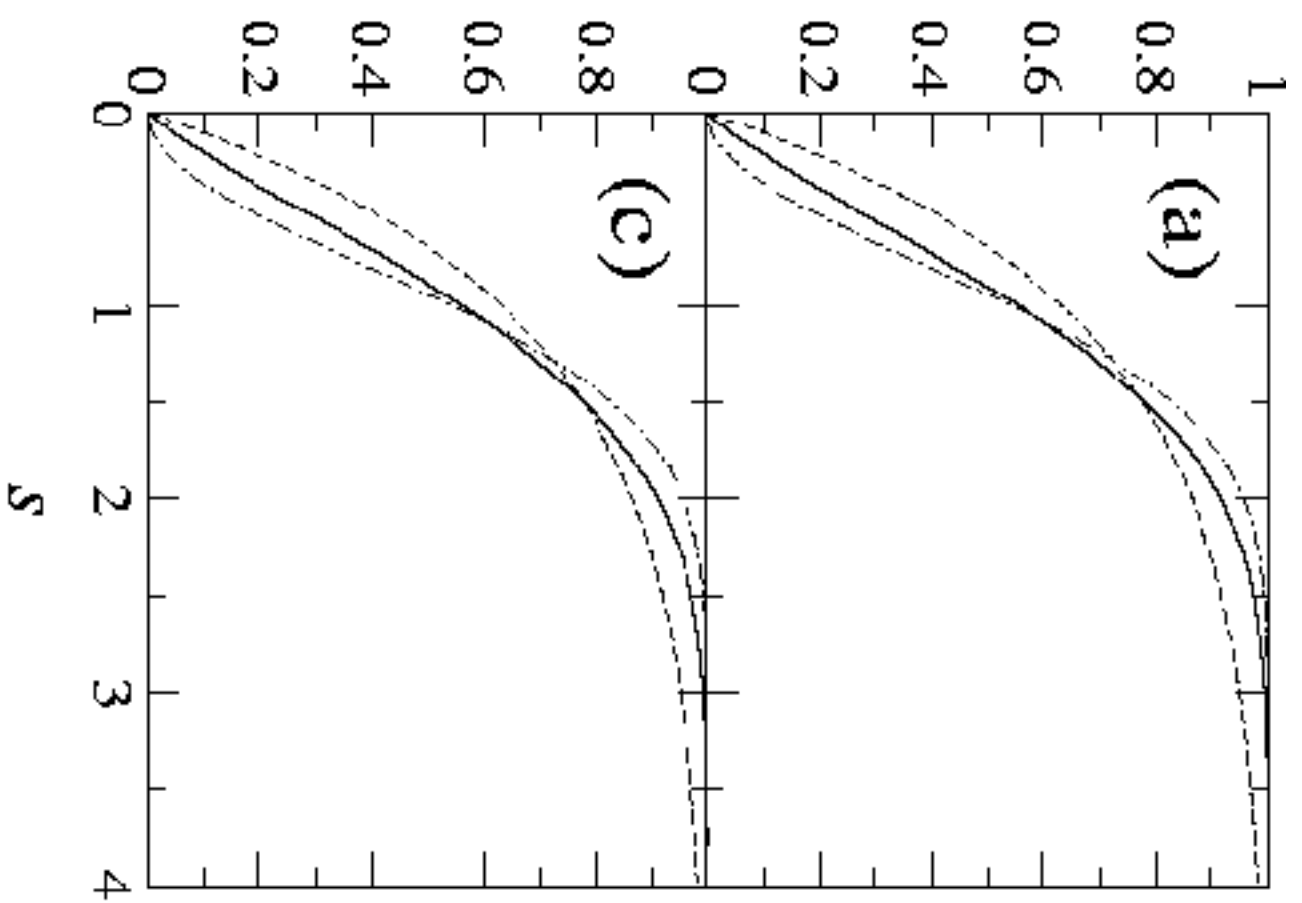
FIG. 11. Nearest neighbor spacing distribution for the hydrogen atom resonantly driven by an elliptically polarized microwave field in the presence of a static field oriented in the direction ($\varphi = 0.4\pi$, $\theta = \pi/4$), such that the generalized time-reversal symmetry is broken. The numerical data correspond to $n_0 = 97 - 102$ (40 000 spacings), the solid line gives the fitted Izrailev distribution. The dash-dotted and dashed lines correspond to GOE and GUE Wigner surmises, respectively. The numerical results clearly show a stronger level repulsion than in the GOE case, a signature of the breaking of any anti-unitary symmetry.

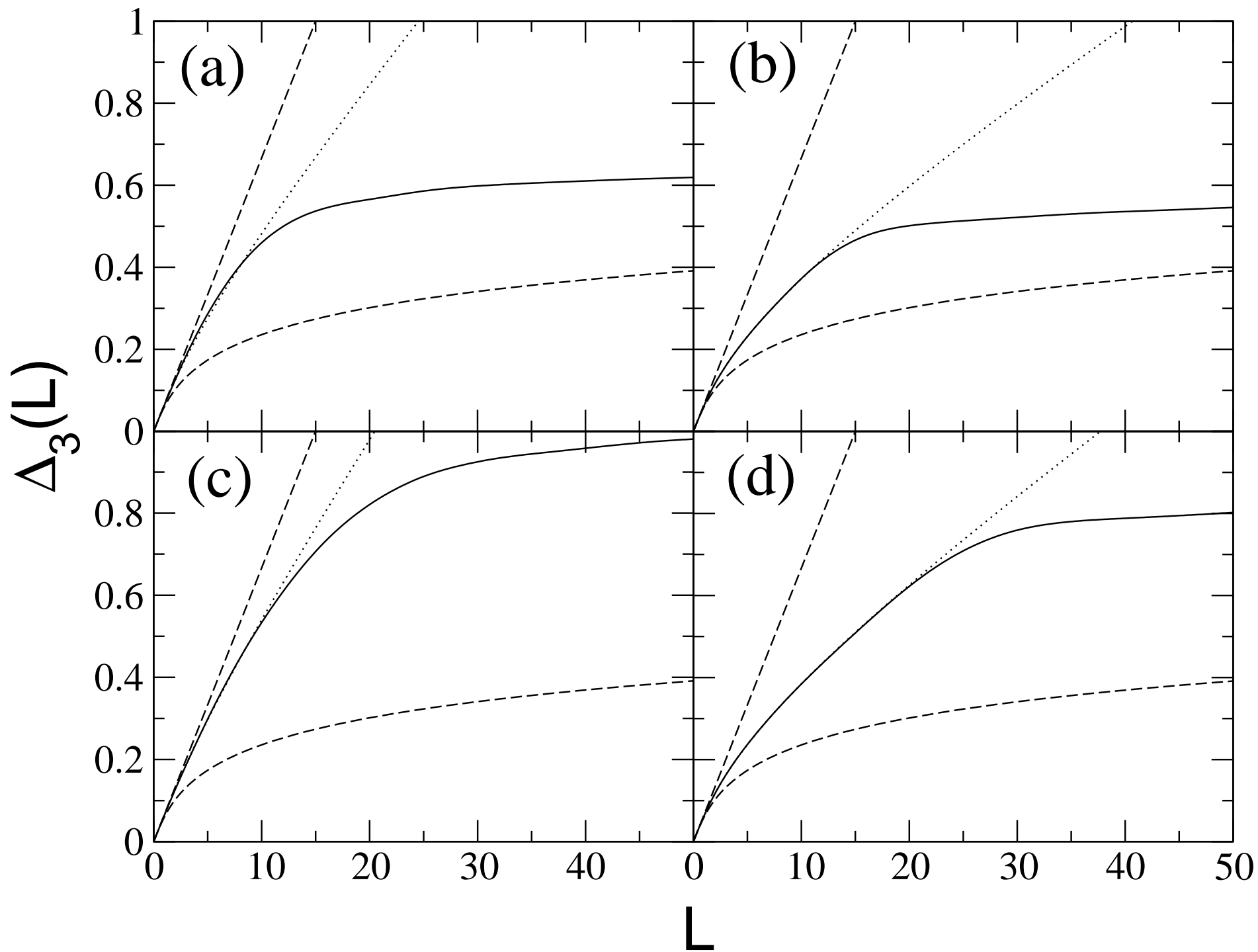


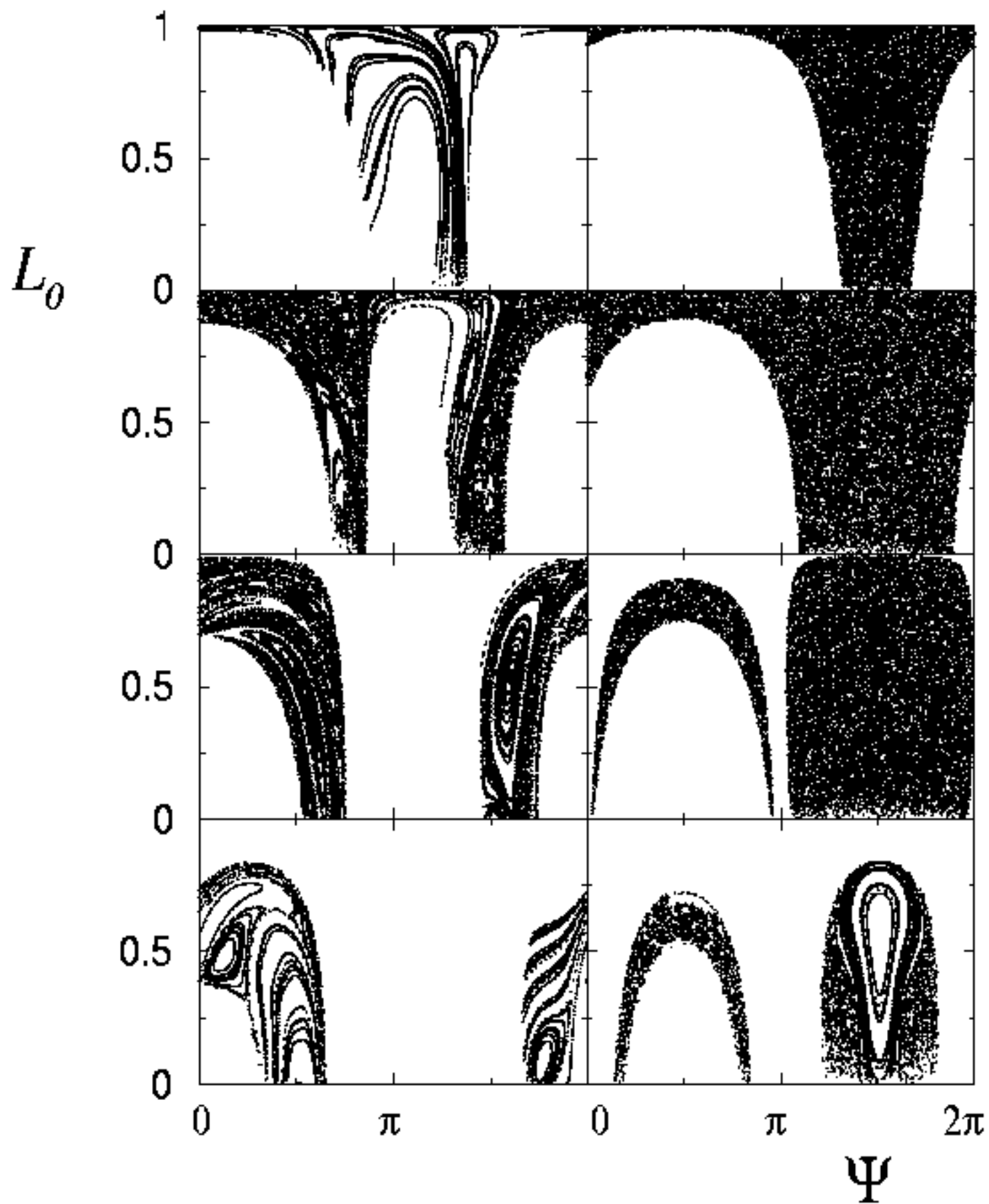


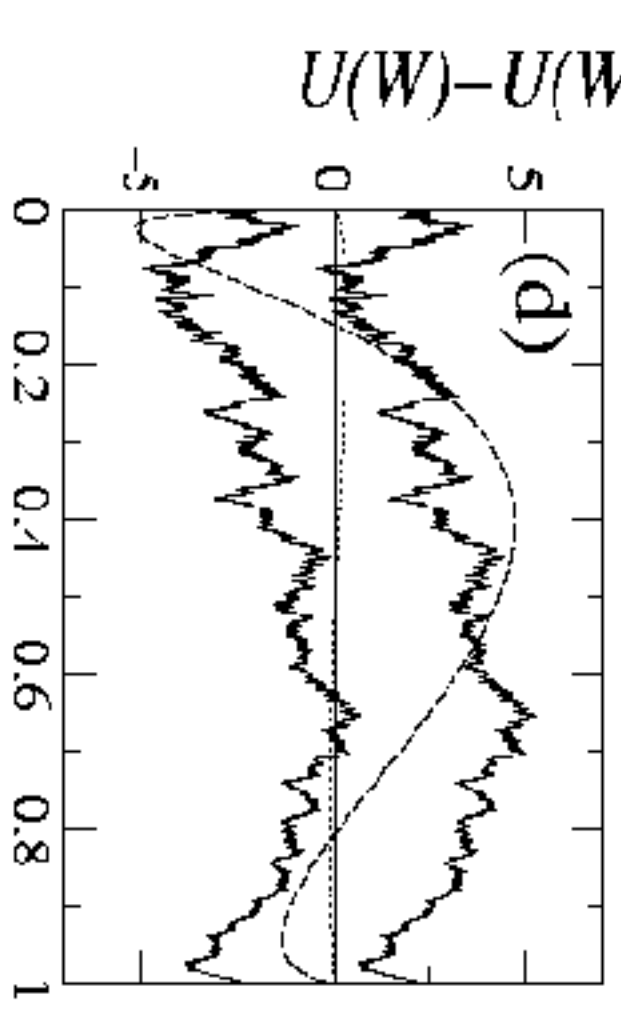
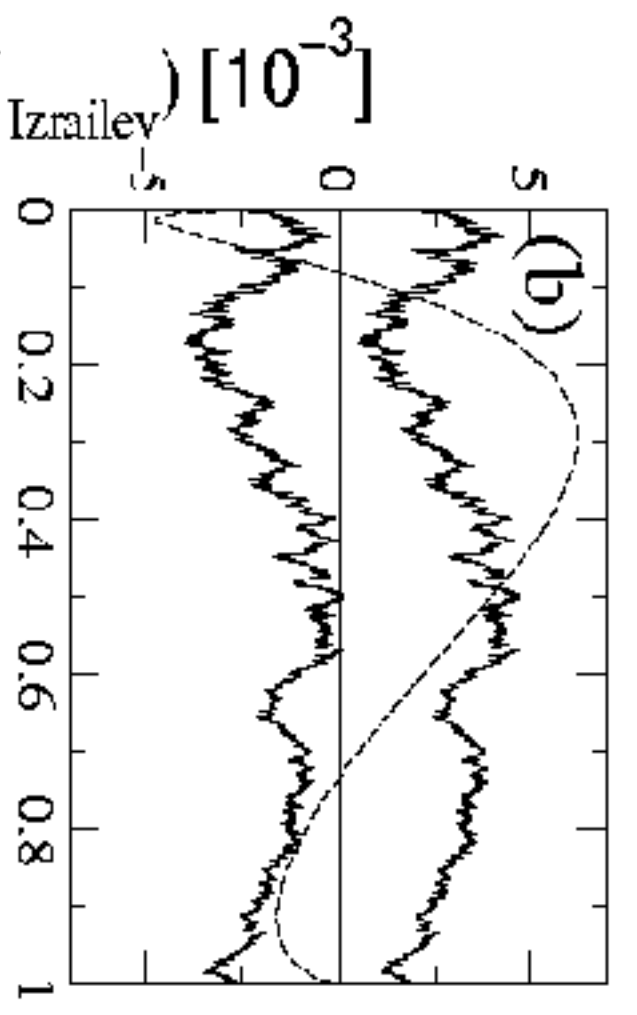
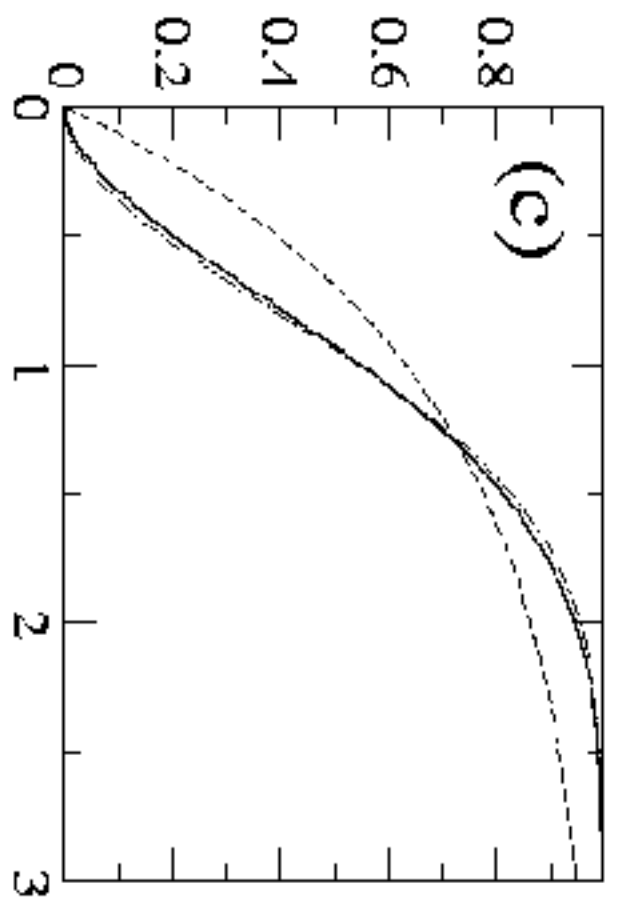
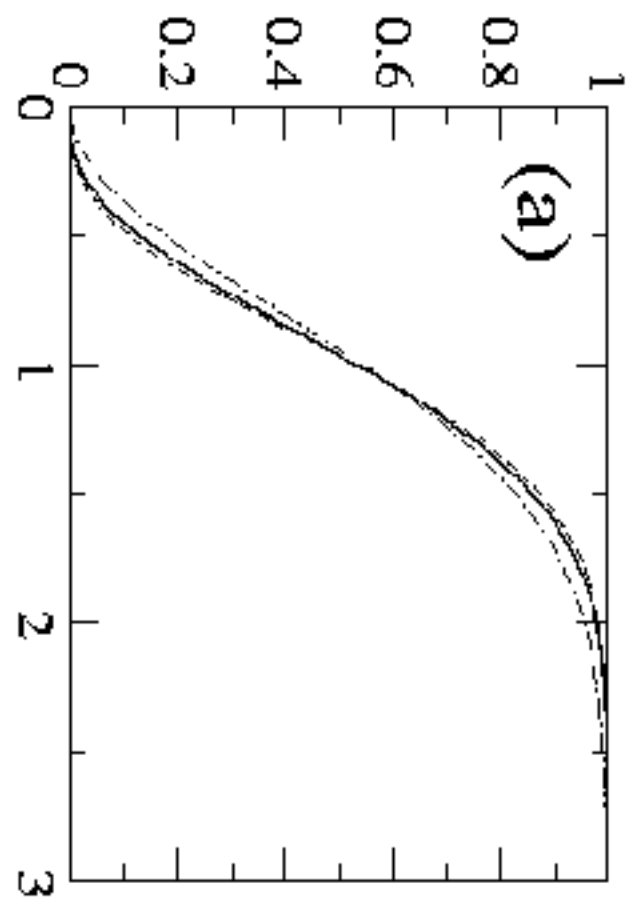












(5)

